

RESEARCH

Open Access



Single cell sequencing analysis identifies genetics-modulated *ORMDL3*⁺ cholangiocytes having higher metabolic effects on primary biliary cholangitis

Bingyu Xiang^{1†}, Chunyu Deng^{2†}, Fei Qiu^{3†}, Jingjing Li⁴, Shanshan Li¹, Huifang Zhang¹, Xiuli Lin¹, Yukuan Huang³, Yijun Zhou³, Jianzhong Su^{3,5}, Mingqin Lu^{1*} and Yunlong Ma^{3*} 

Abstract

Background: Primary biliary cholangitis (PBC) is a classical autoimmune disease, which is highly influenced by genetic determinants. Many genome-wide association studies (GWAS) have reported that numerous genetic loci were significantly associated with PBC susceptibility. However, the effects of genetic determinants on liver cells and its immune microenvironment for PBC remain unclear.

Results: We constructed a powerful computational framework to integrate GWAS summary statistics with scRNA-seq data to uncover genetics-modulated liver cell subpopulations for PBC. Based on our multi-omics integrative analysis, 29 risk genes including *ORMDL3*, *GSNK2B*, and *DDAH2* were significantly associated with PBC susceptibility. By combining GWAS summary statistics with scRNA-seq data, we found that cholangiocytes exhibited a notable enrichment by PBC-related genetic association signals (Permuted $P < 0.05$). The risk gene of *ORMDL3* showed the highest expression proportion in cholangiocytes than other liver cells (22.38%). The *ORMDL3*⁺ cholangiocytes have prominently higher metabolism activity score than *ORMDL3*⁻ cholangiocytes ($P = 1.38 \times 10^{-15}$). Compared with *ORMDL3*⁻ cholangiocytes, there were 77 significantly differentially expressed genes among *ORMDL3*⁺ cholangiocytes ($FDR < 0.05$), and these significant genes were associated with autoimmune diseases-related functional terms or pathways. The *ORMDL3*⁺ cholangiocytes exhibited relatively high communications with macrophage and monocyte. Compared with *ORMDL3*⁻ cholangiocytes, the VEGF signaling pathway is specific for *ORMDL3*⁺ cholangiocytes to interact with other cell populations.

Conclusions: To the best of our knowledge, this is the first study to integrate genetic information with single cell sequencing data for parsing genetics-influenced liver cells for PBC risk. We identified that *ORMDL3*⁺ cholangiocytes with higher metabolism activity play important immune-modulatory roles in the etiology of PBC.

Keywords: Single cell sequencing analysis, GWAS, Risk genes, PBC, *ORMDL3*, Liver cells

*Correspondence: lmq0906@163.com; glb-biotech@zju.edu.cn

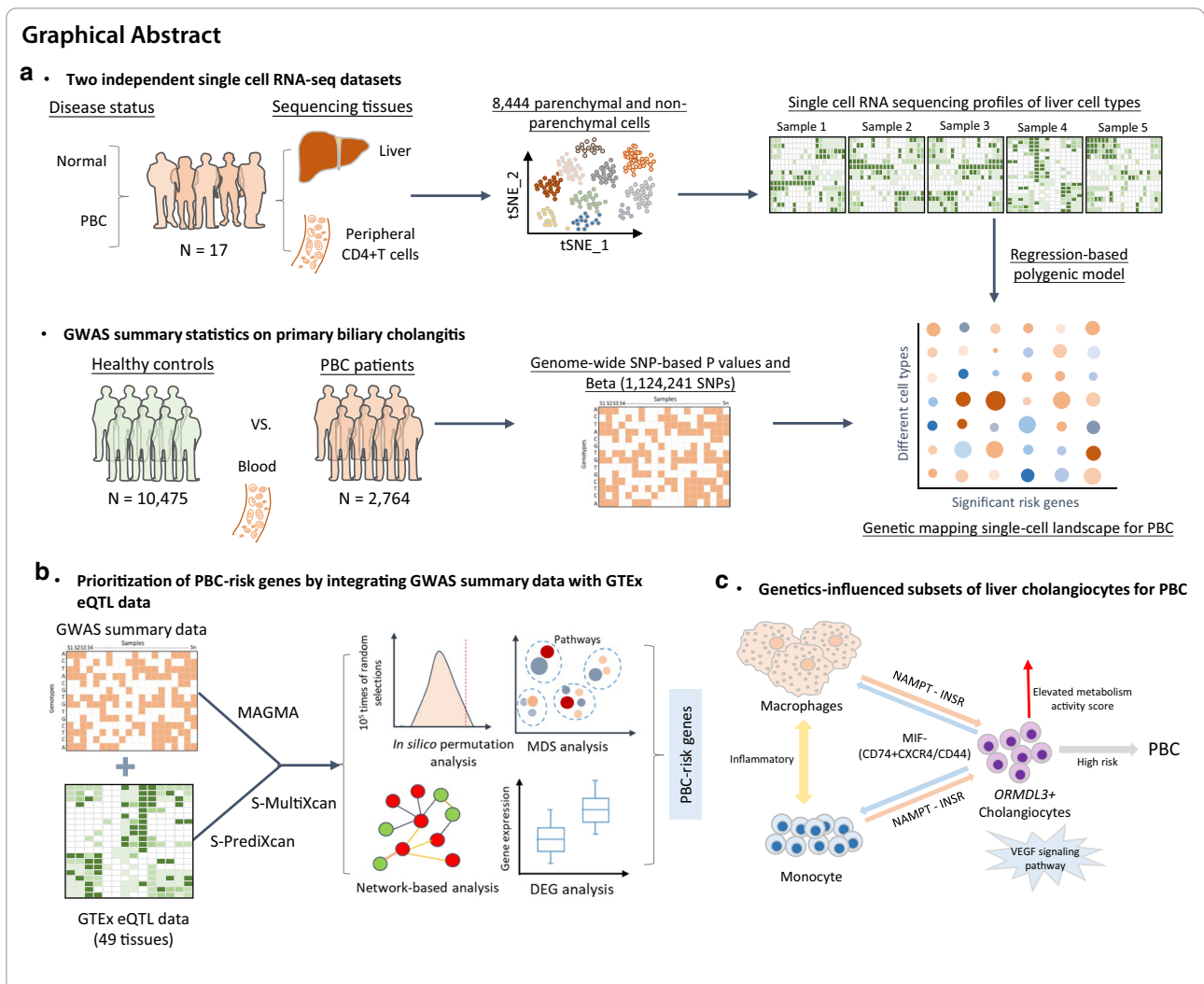
[†]Bingyu Xiang, Chunyu Deng and Fei Qiu contributed equally to this work

¹ Department of Infectious Diseases, The First Affiliated Hospital of Wenzhou Medical University, Wenzhou 325000, Zhejiang, China

³ Institute of Biomedical Big Data, School of Ophthalmology and Optometry and Eye Hospital, School of Biomedical Engineering, Wenzhou Medical University, Wenzhou 325027, Zhejiang, China

Full list of author information is available at the end of the article





Background

Primary biliary cholangitis (PBC), which is formally known as primary biliary cirrhosis until 2016 [1], is a rare chronic cholestatic liver disease characterized by progressive autoimmune-mediated destruction of the small intrahepatic biliary epithelial cells [2, 3]. PBC patients suffering from chronic cholestasis can eventually lead to cirrhosis and hepatic failure without effective treatments [2]. Although ursodeoxycholic acid has been used as the first-line therapeutic agent for PBC, there exist 10–20% of PBC patients resistant to ursodeoxycholic acid and developing to advanced-stage liver disease [2]. Previous studies [4] have reported that a combination of genetic and environmental risk factors have an important influence on the aetiology of PBC. Hence, understanding the genetic mechanisms of PBC is becoming a great interest, which may promote the development of individualized therapeutic strategy for PBC.

Over the past decade, a growing number of genome-wide association studies (GWAS) and Immunochip studies based on East Asian and European populations have been performed to uncover the genetic susceptibility loci associated with PBC [4]. To date, more than 40 genetic loci with numerous risk genes have been reported [5–10], such as *SLC19A3/CCL20*, *IRF8/FOXF1*, *NFKB1/MANBA*, and *PDGFB/RPL3*. Nevertheless, the GWAS approach has generally focused on examining the genetic associations of millions of single nucleotide polymorphisms (SNPs) and only a handful of SNPs with a genome-wide significance ($P \leq 5 \times 10^{-8}$) are reported. There exist many common SNPs with small marginal effects were neglected [11, 12]. Moreover, the vast majority of reported SNPs were mapped within non-coding genomic regions [12]. It is plausible to infer that these non-coding SNPs may modulate the expression levels of corresponding risk genes rather than change the

functions of their proteins. Thus, combination of GWAS summary statistics and other different types of data that characterize tissue- and cell-type-specific activity, including expression quantitative trait loci (eQTL) [11], DNase I-hypersensitive sites (DHS) [13], and histone marks [14], contributes to highlight disease-related risk genes and cell types.

With the advance of single cell sequencing techniques, researchers have an effective avenue to discover more refined and novel cell populations for complex diseases [15]. An accruing and large number of single cell RNA sequencing (scRNA-seq) studies on autoimmune diseases, including rheumatoid arthritis [16], inflammatory bowel disease [17], and systemic lupus erythematosus [18], have been reported to parse the heterogeneity of cellular subpopulations at unprecedented resolution. In view of no scRNA-seq study was conducted for uncovering human liver cell types implicated in PBC, we constructed a computational framework to identify risk genes whose genetically expressions associated with PBC and pinpoint cell subpopulations implicated in the etiology of PBC.

Results

The framework for integrating single-cell transcriptomes and GWAS on PBC

In the current study, we constructed a computational framework to unveil the cell-type specific genetic influence on the etiology of PBC based on multiple omics datasets (Fig. 1 and Additional file 2: Table S1). It included three primary sections: (1) combination of GWAS summary statistics on PBC with scRNA-seq data to recapitulate the genetics-modulated single cell landscape for PBC (Fig. 1a), (2) prioritization of genetics-risk genes and pathways contributing to PBC (Fig. 1b), and (3) revelation of the cell-to-cell interactions and metabolic activities of genetics-influenced subset of liver cholangiocytes and its immune microenvironment for PBC (Fig. 1c).

Identification of gene-level genetic associations for PBC

To identify the aggregated effects of SNPs in a given gene on PBC, we performed a gene-level genetic association analysis and found that 563 genes were significantly associated with PBC ($FDR \leq 0.05$, Additional file 1: Fig. S1, Additional file 2: Table S2). For example, the top-ranked genes of *HLA-DPA1* ($P = 2.69 \times 10^{-24}$), *IL12A* ($P = 6.63 \times 10^{-22}$), and *BTNL2* ($P = 1.65 \times 10^{-17}$). By using a genome-wide pathway analysis, there were 41 KEGG pathways significantly enriched ($FDR \leq 0.05$, Additional file 2: Table S3 and Additional file 1: Fig. S2a). Based on the MDS analysis, these 41 pathways were grouped into five clusters, including Th1 and Th2 cell differentiation,

allograft rejection, Th17 cell differentiation, cell adhesion molecules, and cytokine-cytokine receptor interactions (Additional file 1: Fig. S2b). The top-ranked pathways, such as Th1 and Th2 cell differentiation, allograft rejection, inflammatory bowel disease, and type I diabetes mellitus, were relevant to autoimmune diseases.

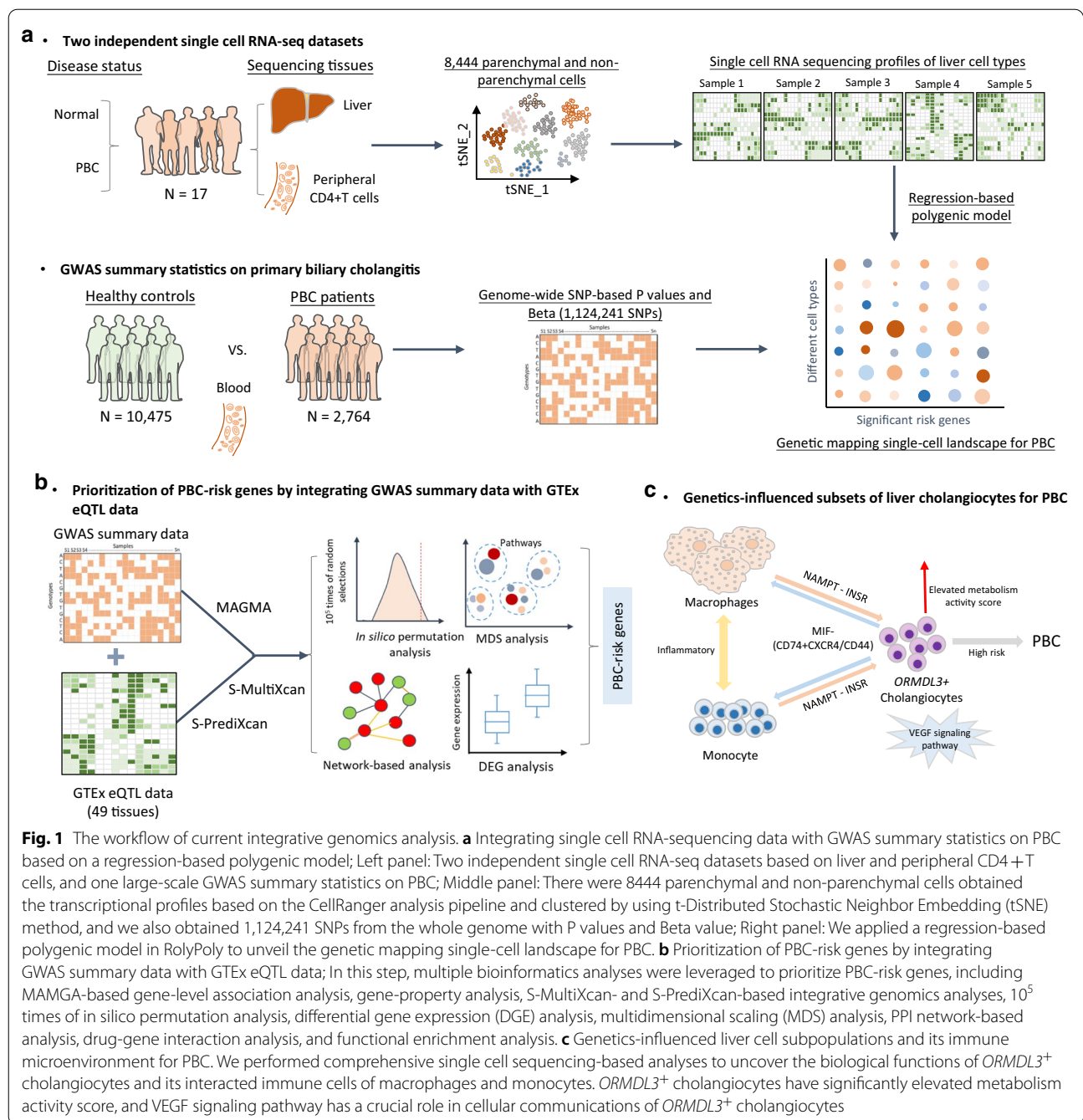
Furthermore, by performing a gene-property analysis based on mouse liver tissue with immune cells, we found that PBC-associated genes were significantly enriched in several immune-related cell types (Additional file 1: Fig. S3 and Additional file 2: Table S4), including *Cst3*⁺ dendritic cell ($P = 5.8 \times 10^{-3}$), *Trbc2*⁺ T cell ($P = 7.1 \times 10^{-3}$), *Chil3*⁺ macrophage ($P = 0.017$), and *Gzma*⁺ T cell ($P = 0.03$), which were in line with the results in previous studies [19, 20].

Integrative analysis of GWAS summary statistics with eQTL data for PBC

To further highlight the functional genes whose expressions are associated with PBC, we leveraged the S-MultiXcan software [21] to meta-analyze tissue-specific associations across 49 GTEx tissues. There were 268 risk genes whose genetically-associated expression showing notable associations with PBC ($FDR \leq 0.05$, Fig. 2). Among these significant genes, there were 52 risk genes having been documented in the GWAS Catalog database (Additional file 2: Table S5). Moreover, there was a high consistency of results between MAGMA and S-MultiXcan analysis ($232/268 = 86.6\%$, Additional file 1: Fig. S4), such as *HLA-DRB1* ($P = 4.95 \times 10^{-69}$), *HLA-DRB5* ($P = 1.17 \times 10^{-42}$), and *BTNL2* ($P = 3.26 \times 10^{-41}$).

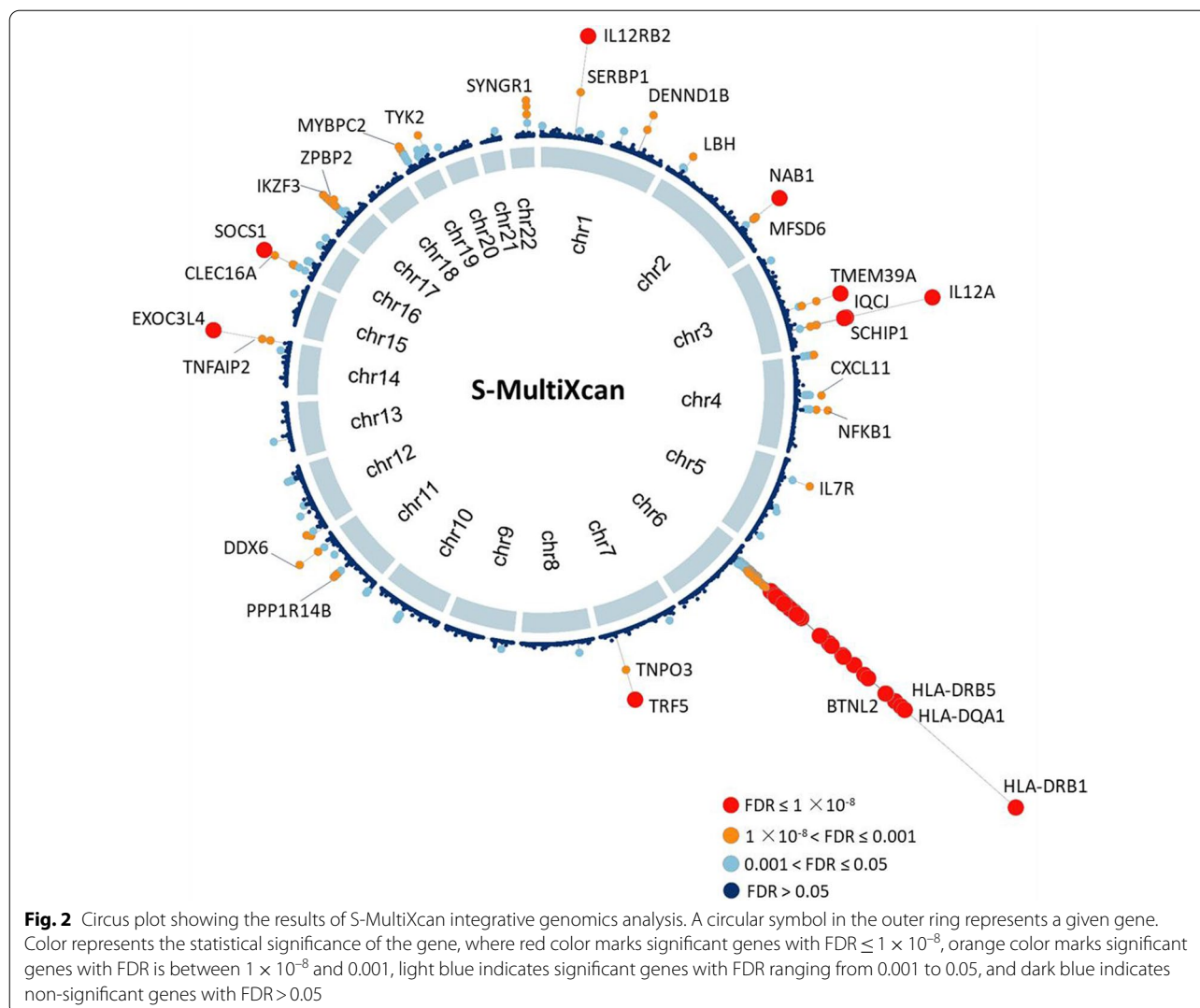
To further validate these risk genes in two PBC-relevant tissues (i.e., liver and blood) using the S-PrediXcan method, we found that 76 and 115 genes were significantly associated with PBC in liver and blood, respectively ($FDR \leq 0.05$, Fig. 3a, b and Additional file 2: Tables S6, S7). In total, 29 risk genes were significantly associated with PBC across different methods including MAGMA, S-MultiXcan, and S-PrediXcan analyses (Fig. 3c). Using the Pearson correlation analysis, we observed that significant genes from S-MultiXcan analysis showed remarkable correlations with that from MAGMA and S-PrediXcan analyses ($P \leq 0.05$, Fig. 3d–f). Moreover, by performing three independent permutation analyses, we found that the number of observed overlapped genes between S-MultiXcan and MAGMA and S-PrediXcan were significantly higher than random events (Empirical $P < 1 \times 10^{-5}$, Fig. 3g–i and Additional file 1: Fig. S5a–c). Overall, we identified 29 genes contribute susceptibility to PBC (Table 1).

Based on three independent expression profiles of liver, blood, and peripheral CD4⁺ T cells, we conducted differential gene expression analysis for these 29 risk genes



between PBC and matched control group. We found that 23 of 29 genes (79.31%) showed significantly differential expressions in PBC patients compared with controls (Table 1 and Additional file 1: Figures S6–S8). The co-expression patterns among these 29 genes in the peripheral CD4 + T cells were prominently altered according to the PBC status (Additional file 1: Fig. S8a). These results further support these identified risk genes have crucial effects on PBC.

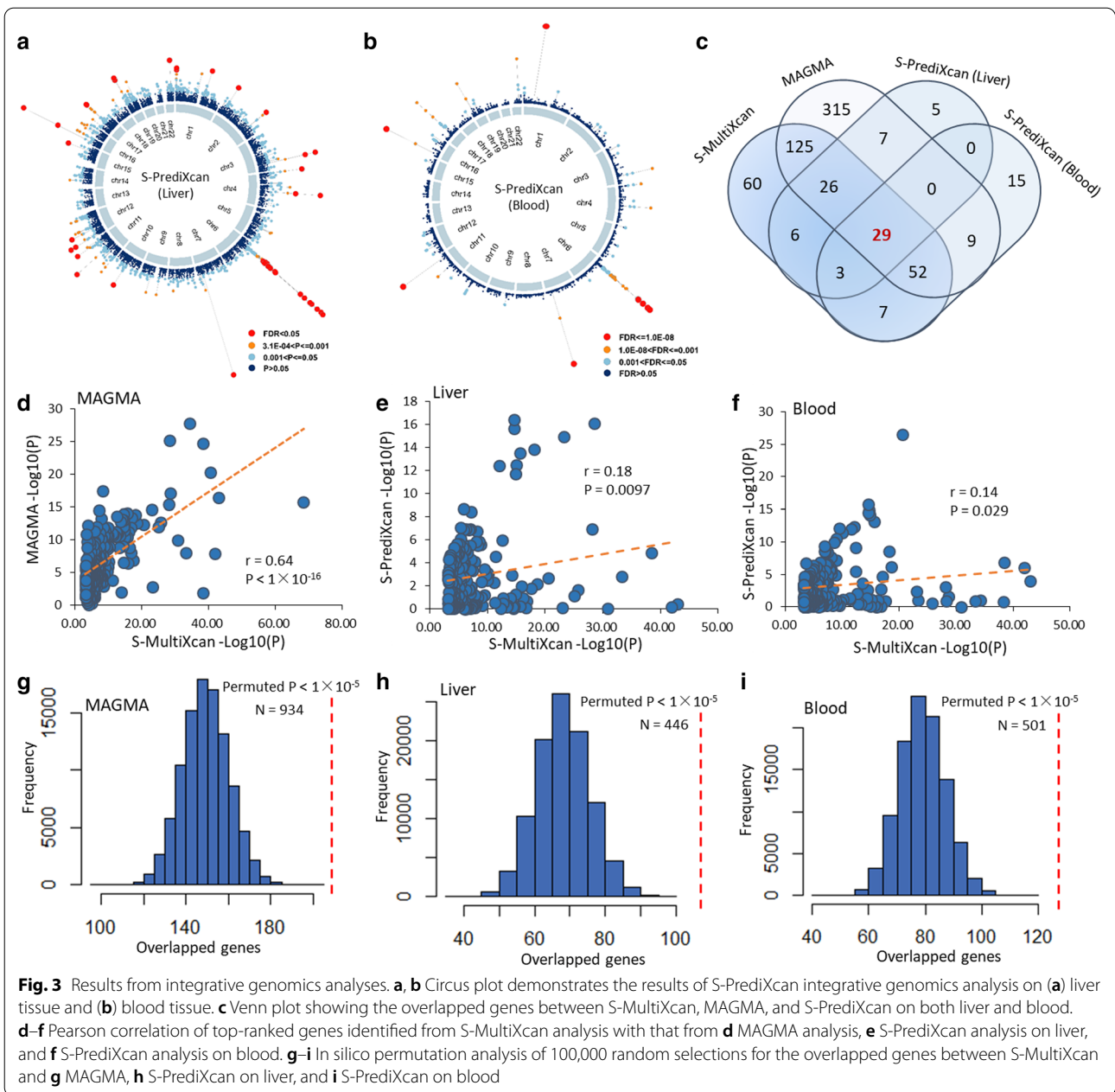
Functional analysis of these 29 PBC-associated risk genes
 Through mining the PubMed literature and GWAS Catalog database, we found that 10 of 29 identified risk genes have been reported to be associated with PBC in previous GWAS studies, and there were 19 novel genes newly identified (Table 1 and Additional file 1: Fig. S9a). Among these novel identified genes, several genes (e.g., *LY6G5B* and *DDAH2*) were associated with autoimmune-related diseases, including rheumatoid arthritis [22] and type 1



diabetes [23]. By conducting a PPI network enrichment analysis, we observed that these risk genes were significantly interacted with each other in a subnetwork (Fig. 4). For example, *TCF19* showed shared protein domains with *IRF5* [24], and *DDAH2* was highly co-expressed with *CSNK2B* [25].

Furthermore, we performed a phenotype-based enrichment analysis, and found that these 29 risk genes were remarkably enriched in several phenotypes relevant to autoimmune diseases ($FDR \leq 0.05$, Additional file 1: Fig. S9b and Additional file 2: Table S8), such as type I diabetes mellitus, immune system diseases, and juvenile rheumatoid arthritis. We also performed a GO-term enrichment analysis, and found that several GO-terms were notably overrepresented (Additional file 1: Figs. S10–S12), such as interferon-gamma-mediated signaling pathway ($P = 2.8 \times 10^{-4}$) and neutrophil activation involved in immune response ($P = 7.3 \times 10^{-4}$).

Based on the drug-gene interaction analysis, we identified that 20 of 29 genes (68.96%) were enriched in ten potential “druggable” gene categories (Additional file 1: Fig. S13a and Additional file 2: Table S9). Five genes including *SOCS1*, *TCF19*, *CARM1*, *SH2B3*, and *NAAA* were directly targeted at least one known drug (Additional file 1: Fig. S13b). The gene of *SOCS1* was found to be targeted by insulin and aldesleukin, of which both have been applied to treat autoimmune diseases, including systemic lupus erythematosus [26], type 1 diabetes mellitus [27], and HIV [28]. *SH2B3* was targeted by ruxolitinib and candesartan. Previous studies [29] have demonstrated that the Janus kinase (JAK)-inhibitor ruxolitinib significantly influenced dendritic cell differentiation and function resulting in impaired T-cell activation, which could be used for the treatment of autoimmune diseases. These results provide a good drug repurposing resource to develop effective therapeutics for PBC.



Identification of genetically-influenced liver cell subpopulations for PBC

Using the uniform manifold approximation and projection (UMAP), there were 22 discrete clusters for the liver scRNA-seq dataset (Fig. 5a). Using well-known marker genes, these clusters were assigned into 13 distinct cell subpopulations, including portal endothelial cells, cholangiocytes, non-inflammatory macrophages, T cells, $\gamma\delta$ T cells, inflammatory monocytes/macrophages, natural killer (NK)-like cells, red blood cells (RBCs), sinusoidal endothelial cells, mature B cells, stellate cells,

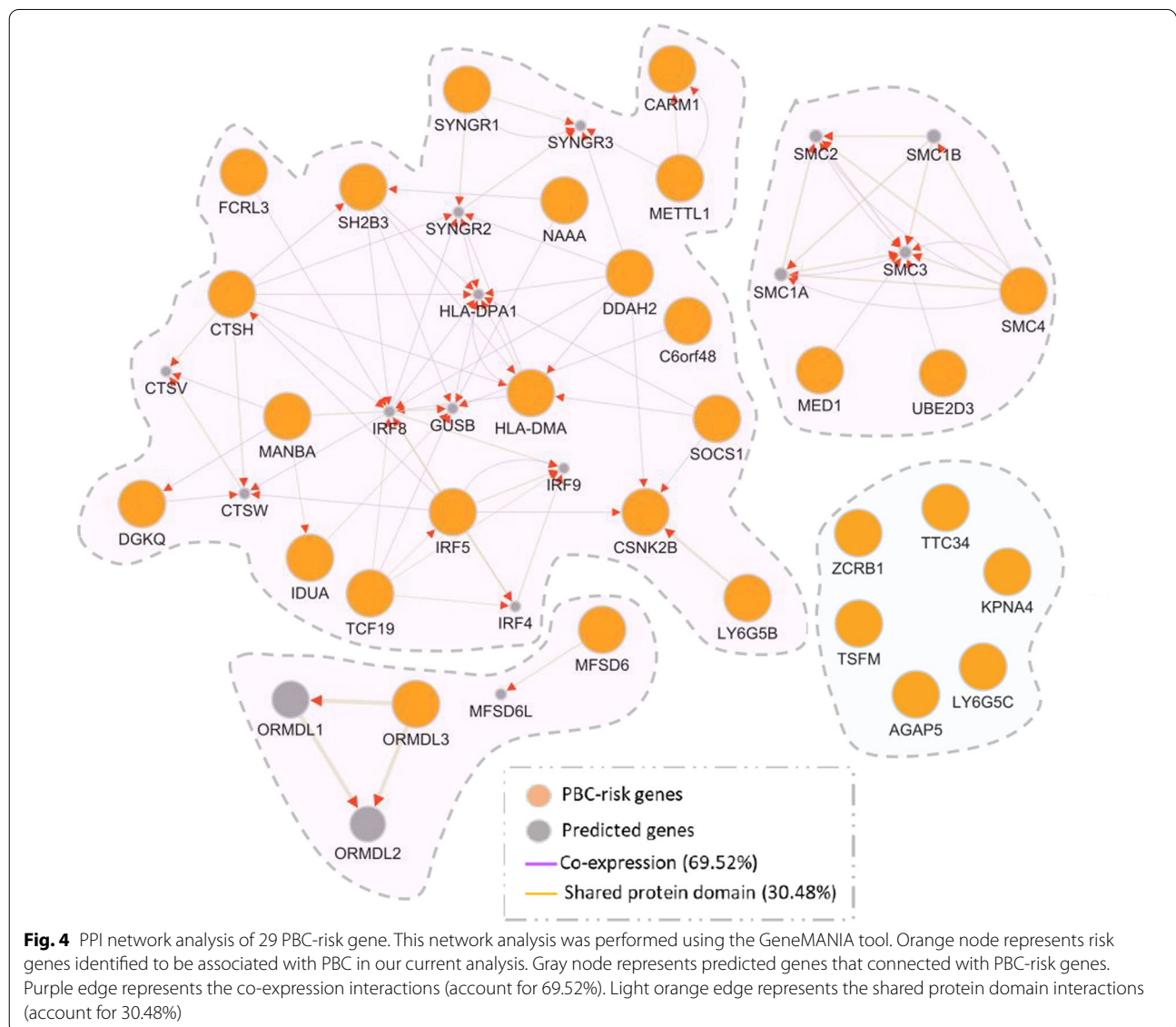
plasma cells, and hepatocytes (Fig. 5b). By calculating the genetic risk score of 29 PBC-associated genes using the *AddModuleScore* function in Seurat, we found that these risk genes were primarily enriched in non-inflammatory macrophage and inflammatory monocyte/macrophage (Fig. 5c), suggesting that these risk genes may have crucial functions in innate immunity for PBC. To uncover genetics-regulatory cell subpopulations associated with PBC, we used a regression-based polygenic model to combine GWAS summary statistics on PBC with scRNA-seq data with 13 distinct human liver cell types. We

Table 1 Identification of 29 significant risk genes by using integrative genomics analysis

Gene name	Z score	P value (S-MultiXcan)	FDR (S-MultiXcan)	FDR (S-PrediXcan on liver)	FDR (S-PrediXcan on blood)	FDR (MAGMA analysis of GWAS)	P value (Differential gene expression analysis)	GWAS_Catalog database or PubMed database
<i>CSNK2B</i>	1.40	7.17×10^{-19}	8.41×10^{-16}	3.22×10^{-11}	2.24×10^{-6}	1.67×10^{-11}	4.96×10^{-4} (Blood), 2×10^{-2} (CD14+T cell)	Novel gene
<i>LY6G5B</i>	- 7.92	2.43×10^{-16}	1.93×10^{-13}	5.52×10^{-11}	1.54×10^{-10}	1.19×10^{-11}	Non-significant	Novel gene
<i>DDAH2</i>	- 5.57	1.39×10^{-15}	9.99×10^{-13}	2.65×10^{-9}	1.56×10^{-11}	1.69×10^{-9}	2.70×10^{-3} (CD14+T cell)	Novel gene
<i>LY6G5C</i>	- 7.82	2.40×10^{-15}	1.62×10^{-12}	8.64×10^{-13}	9.05×10^{-12}	1.41×10^{-11}	2.80×10^{-2} (Blood)	Novel gene
<i>IRF5</i>	7.11	2.62×10^{-15}	1.72×10^{-12}	4.29×10^{-13}	1.12×10^{-12}	7.18×10^{-11}	7.10×10^{-3} (Liver)	Reported gene
<i>SOCS1</i>	- 3.26	9.33×10^{-13}	4.16×10^{-10}	5.25×10^{-10}	7.34×10^{-10}	1.06×10^{-8}	3.50×10^{-2} (CD14+T cell)	Reported gene
<i>SYNGR1</i>	- 1.30	2.83×10^{-9}	8.88×10^{-7}	7.97×10^{-4}	1.30×10^{-7}	4.13×10^{-2}	1.40×10^{-2} (CD14+T cell)	Reported gene
<i>C6orf48</i>	- 4.46	9.57×10^{-9}	2.66×10^{-6}	7.83×10^{-4}	6.19×10^{-4}	4.83×10^{-11}	4.16×10^{-6} (Blood)	Novel gene
<i>HLA-DMA</i>	- 3.99	8.87×10^{-8}	1.90×10^{-5}	1.27×10^{-3}	9.16×10^{-4}	1.62×10^{-8}	2.10×10^{-3} (Liver)	Novel gene
<i>SMC4</i>	- 1.34	1.00×10^{-7}	2.10×10^{-5}	9.38×10^{-5}	2.25×10^{-6}	2.07×10^{-4}	4.80×10^{-4} (Blood)	Novel gene
<i>TCF19</i>	4.55	1.49×10^{-7}	2.99×10^{-5}	9.46×10^{-5}	2.24×10^{-6}	1.98×10^{-4}	Non-significant	Novel gene
<i>ORMDL3</i>	- 2.92	7.07×10^{-7}	1.22×10^{-4}	2.35×10^{-3}	7.38×10^{-5}	2.33×10^{-6}	3.5×10^{-2} (Liver)	Reported gene
<i>KPNA4</i>	- 1.22	1.07×10^{-6}	1.82×10^{-4}	2.10×10^{-2}	3.58×10^{-3}	4.67×10^{-4}	3.40×10^{-3} (CD14+T cell)	Novel gene
<i>MANBA</i>	- 1.45	1.48×10^{-6}	2.35×10^{-4}	2.46×10^{-6}	2.39×10^{-2}	8.30×10^{-8}	9.67×10^{-5} (Blood)	Reported gene
<i>MFSD6</i>	- 0.32	1.61×10^{-6}	2.51×10^{-4}	2.55×10^{-2}	4.57×10^{-2}	2.06×10^{-3}	3.60×10^{-2} (Liver)	Novel gene
<i>MED1</i>	- 2.13	1.76×10^{-6}	2.70×10^{-4}	1.65×10^{-2}	1.53×10^{-2}	4.42×10^{-5}	Non-significant	Novel gene
<i>IDUA</i>	3.95	2.37×10^{-6}	3.47×10^{-4}	3.94×10^{-2}	3.87×10^{-2}	8.95×10^{-4}	8.10×10^{-3} (Blood)	Reported gene
<i>DGKQ</i>	3.24	3.86×10^{-6}	5.37×10^{-4}	4.90×10^{-4}	3.36×10^{-4}	2.35×10^{-4}	8.34×10^{-7} (Blood)	Reported gene
<i>FCRL3</i>	- 4.40	8.14×10^{-6}	1.07×10^{-3}	2.84×10^{-3}	2.84×10^{-3}	5.81×10^{-4}	Non-significant	Reported gene
<i>ZCRB1</i>	3.22	9.34×10^{-6}	1.20×10^{-3}	4.83×10^{-3}	5.02×10^{-3}	1.52×10^{-3}	5.90×10^{-3} (Liver); 2.8×10^{-3} (CD14+T cell);	Novel gene
<i>AGAP5</i>	- 4.28	1.29×10^{-5}	1.59×10^{-3}	4.50×10^{-3}	3.40×10^{-3}	3.65×10^{-2}	Non-significant	Novel gene
<i>CARM1</i>	- 2.90	2.11×10^{-5}	2.49×10^{-3}	1.14×10^{-3}	8.92×10^{-4}	1.86×10^{-4}	2.60×10^{-2} (Blood)	Novel gene
<i>UBE2D3</i>	- 4.18	2.83×10^{-5}	3.23×10^{-3}	2.76×10^{-3}	5.08×10^{-3}	5.81×10^{-4}	3.40×10^{-2} (Blood); 1.6×10^{-4} (CD14+T cell)	Novel gene
<i>NAAA</i>	4.08	6.73×10^{-5}	6.88×10^{-3}	1.25×10^{-2}	6.85×10^{-3}	7.41×10^{-4}	3.20×10^{-2} (Liver)	Reported gene
<i>SH2B3</i>	- 1.69	1.20×10^{-4}	1.17×10^{-2}	2.35×10^{-2}	1.87×10^{-2}	2.44×10^{-3}	1.40×10^{-2} (Blood)	Reported gene
<i>CTSH</i>	1.75	2.05×10^{-4}	1.84×10^{-2}	8.53×10^{-3}	3.46×10^{-2}	2.19×10^{-5}	Non-significant	Novel gene
<i>TTC34</i>	3.56	2.82×10^{-4}	2.39×10^{-2}	5.86×10^{-3}	5.02×10^{-3}	4.98×10^{-3}	9.80×10^{-3} (Blood)	Novel gene
<i>METTL1</i>	2.19	3.11×10^{-4}	2.59×10^{-2}	4.95×10^{-2}	3.81×10^{-2}	1.68×10^{-2}	5.86×10^{-7} (Blood)	Novel gene

Table 1 (continued)

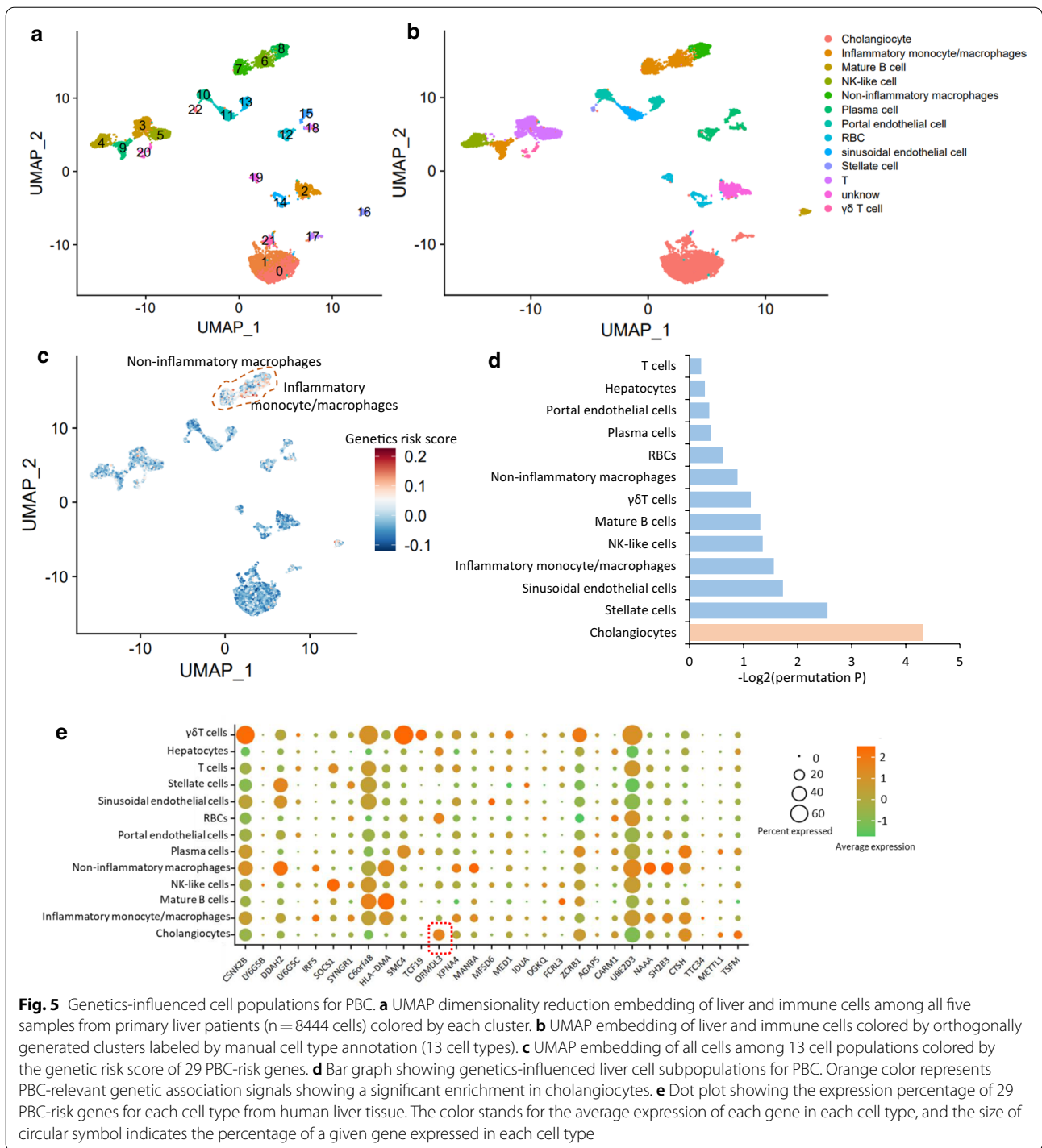
Gene name	Z score	P value (S-MultiXcan)	FDR (S-MultiXcan)	FDR (S-PrediXcan on liver)	FDR (S-PrediXcan on blood)	FDR (MAGMA analysis of GWAS)	P value (Differential gene expression analysis)	GWAS_Catalog database or PubMed database
<i>TSFM</i>	3.45	3.14×10^{-4}	2.61×10^{-2}	4.87×10^{-2}	3.87×10^{-2}	1.54×10^{-2}	2.80×10^{-4} (Blood); 1.5×10^{-3} (CD14+T cell)	Novel gene



found that cholangiocytes showed a notable enrichment by PBC-relevant genetic association signals (Permuted $P < 0.05$, Fig. 5d and Additional file 2: Table S10). These results are consistent with previous evidence that an

immune-mediated injury of cholangiocytes contributes risk to PBC [30, 31].

Using the specificity algorithm in the MAGMA method [32], we noticed that the risk gene of *ORMDL3* exhibited



the highest expression in cholangiocytes than other cell types (Fig. 5e and Additional file 2: Table S11). The majority of *ORMDL3*-expressing cells were cholangiocytes with a relative high percentage of 22.38%, reminding that *ORMDL3* was demonstrated to be significantly associated with PBC in earlier studies [7, 9, 33]. Based

on the liver expression profiles generated from healthy mice (n=4) and mice suffering from cholangitis (n=6) from the GEO database (GSE179993), we performed a differential gene expression analysis and found that the *ORMDL3* gene was significantly higher expressed among cholangitis-affected mice than that among healthy

age- and sex-matched mice ($P=0.036$, Additional file 1: Fig. S14). By further performing immunohistochemistry experiment, we observed that the expression of *ORMDL3* in liver tissues of PBC patients was higher than that in the normal liver, which is in line with the results from our genomics analysis (Additional file 1: Fig. S15). The top-ranked risk SNP associated with *ORMDL3* is rs9303277 ($P=2.57 \times 10^{-11}$). This SNP showed significant cell-specific eQTL of *ORMDL3* among naïve B cell ($P=5.8 \times 10^{-10}$), TFH⁺CD4⁺T cell ($P=3.8 \times 10^{-9}$), CD56^{dim} CD16⁺ NK cells ($P=4.4 \times 10^{-9}$), TH1⁺ CD4⁺ T cells ($P=6.0 \times 10^{-6}$), and memory TREG⁺ CD4⁺ T cells ($P=1.1 \times 10^{-5}$), and exhibited notable cell-specific promoter-interacting eQTL of *ORMDL3* among naïve B cell ($P=4.2 \times 10^{-13}$) and CD56^{dim} CD16⁺ NK cells ($P=5.0 \times 10^{-12}$) (Additional file 1: Fig. S16). Among these immune cell types, the CC genotype of rs9303277 shows prominent association with higher expression of *ORMDL3* compared with other genotypes (Additional file 1: Fig. S16a–k).

Growing attentions have concentrated on the role of *ORMDL3* in the development of inflammatory diseases including PBC [7, 9, 34]. In view of the main goal of current study was to characterize genetics-modulated liver cell subpopulations for PBC, the majority of our subsequent analyses focused on revealing the functions of *ORMDL3*⁺ cholangiocytes and its cellular communications with immune cells.

Characterization of biological functions of *ORMDL3*⁺ cholangiocytes

The subset of *ORMDL3*⁺ cholangiocytes account for 22.38% (635/2837) of cholangiocytes (Fig. 6a). By calculating the metabolism activity score among all annotated cells, we found that the cholangiocytes showed remarkably higher metabolism activity score than other cells (Fig. 6b). Interestingly, we noticed that the metabolism activity score of *ORMDL3*⁺ cholangiocytes was significantly higher than that in *ORMDL3*⁻ cholangiocytes ($P=1.383 \times 10^{-15}$, Fig. 6c). Furthermore, we compared the expression profiles of *ORMDL3*⁺ cholangiocytes with *ORMDL3*⁻ cholangiocytes. There were 77 significantly DEGs with six up-regulated DEGs and 71 down-regulated DEGs among *ORMDL3*⁺ cholangiocytes ($FDR<0.05$, Fig. 6d and Additional file 2: Tables S12–S13). With regard to six up-regulated DEGs, there were seven significant pathways overrepresented ($FDR<0.05$, Additional file 1: Fig. S17a and Additional file 2: Table S14).

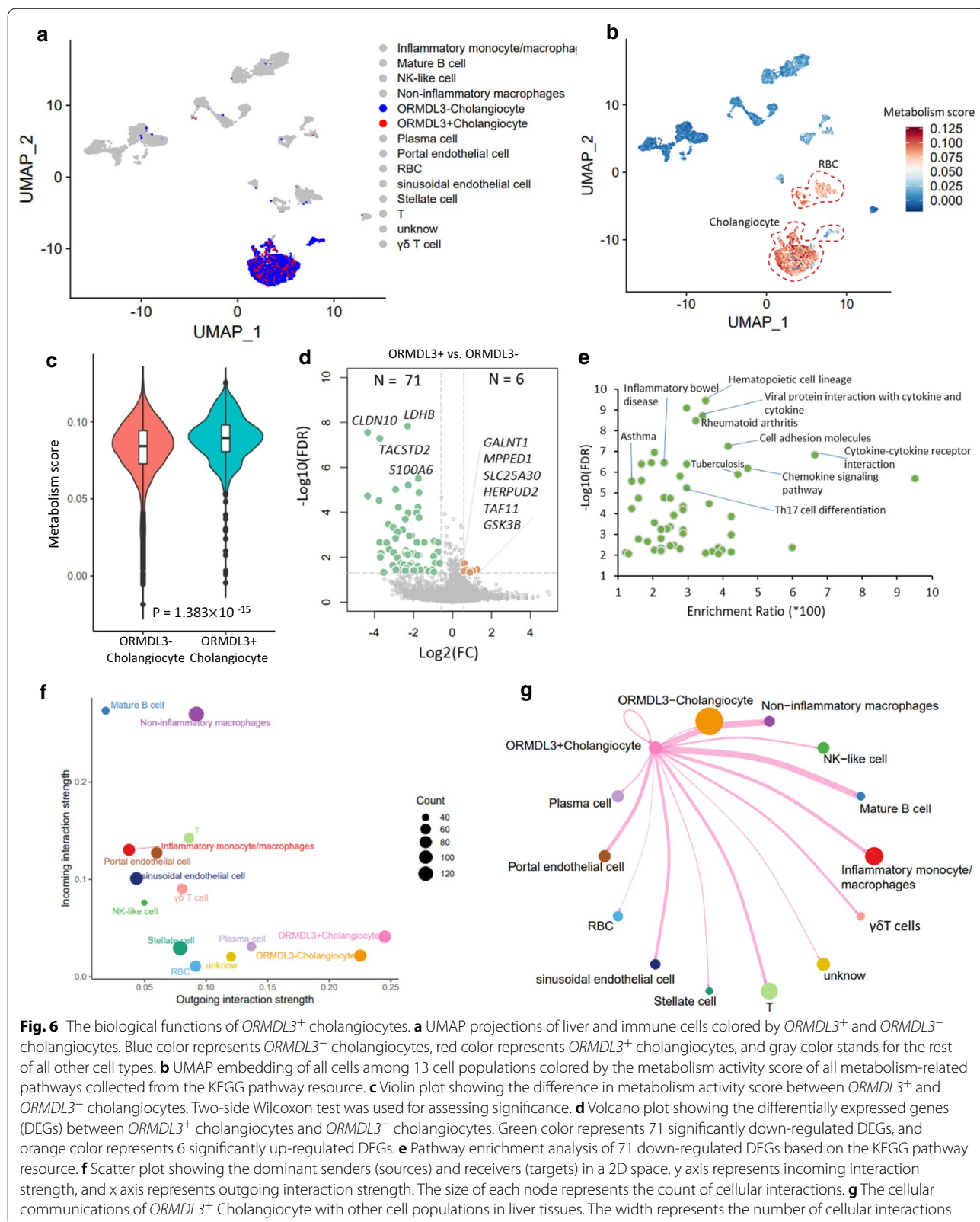
Among the 71 down-regulated DEGs, *HLA-DRA* has been shown to be associated with PBC [7], and *CXCL8*, *CCL3*, *CXCL1*, *TIMP1*, *SPPI1*, and *IRF1* were

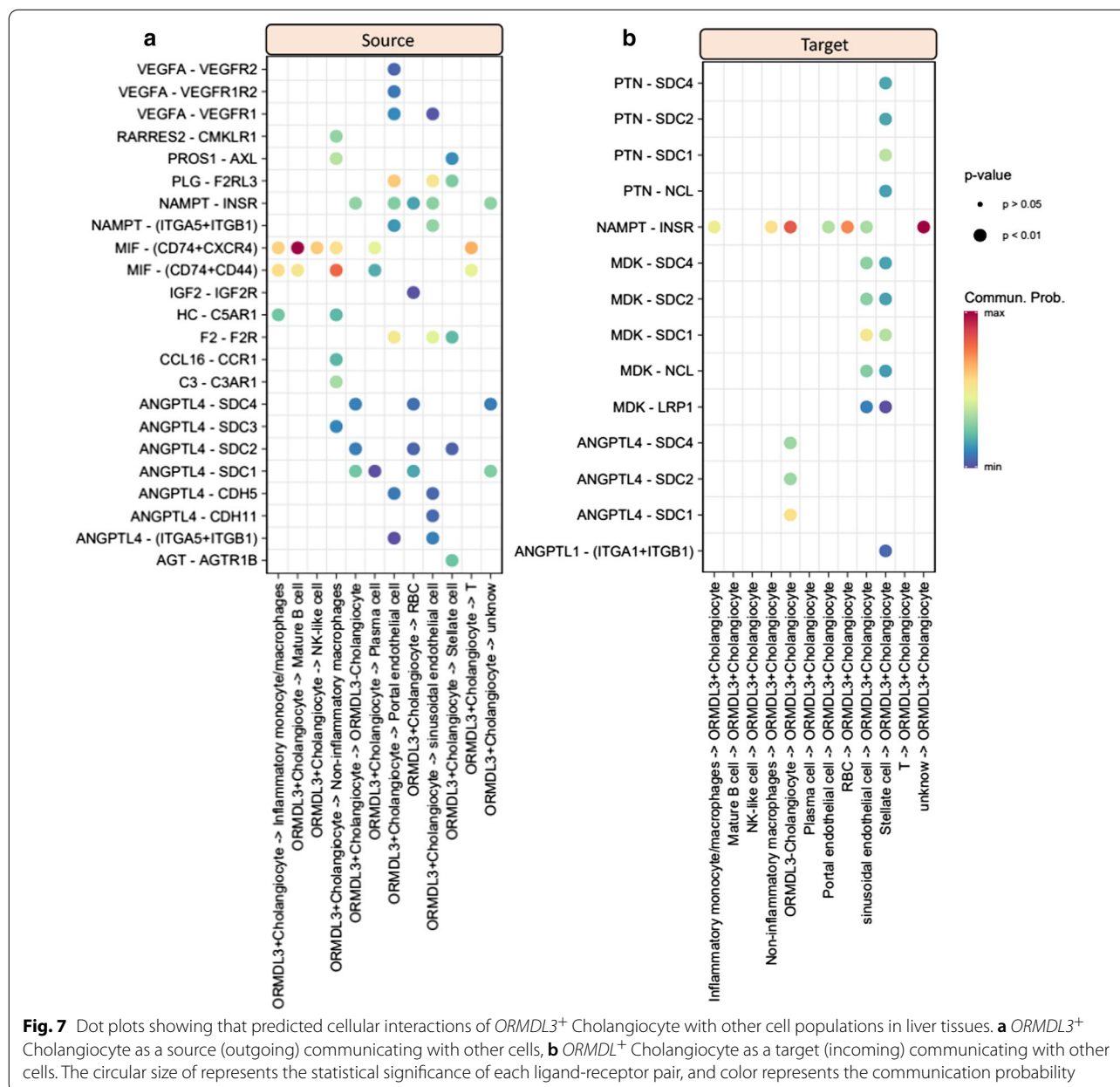
inflammatory and cytokine genes, which have been reported to be linked with the chemotaxis of immune cells that efflux to the site of cytokine storms in response to ongoing tissue damage [35, 36]. *IFI16* is reported to be an innate immune sensor for intracellular DNA [37]. Pathway enrichment analysis revealed that there were 55 significant KEGG pathways enriched by these 71 down-regulated DEGs ($FDR<0.05$, Fig. 6e and Additional file 2: Table S15), of which several such as inflammatory bowel disease, rheumatoid arthritis, Th17 cell differentiation, cytokine-cytokine receptor interaction, and chemokine signaling pathway have been demonstrated to implicate in inflammatory-related diseases [11, 38, 39].

To further explore the biological functions of these 71 down-regulated DEGs, we conducted GO-term enrichment analysis according to three categories of biological process (BP), cellular component (CC), and molecular function (MF). There were 19 BP-terms, 7 CC-terms, and 13 MF-terms showing notable enrichments, respectively ($FDR<0.05$, Additional file 1: Fig. S17b–d and Additional file 2: Tables S16–S18). These functional terms were largely linked with immune and metabolism functions, such as granulocyte activation, neutrophil mediated immunity, and S100 protein binding. These results suggest that *ORMDL3*⁺ cholangiocytes have immune-modulatory effects on PBC risk.

Cellular communications of *ORMDL3*⁺ cholangiocytes with other cells

To gain refined insights into *ORMDL3*⁺ cholangiocytes, we performed a cell-to-cell interaction analysis among cell populations in liver tissue using the CellChat algorithm. By calculating the aggregated cell–cell communication network by counting the number of links, we found that *ORMDL3*⁺ cholangiocytes showed the highest outgoing (sources) interaction strength than other cell types (Fig. 6e and Additional file 1: Fig. S18). By further summarizing the communication probability among cellular interactions, we observed a high connective network of *ORMDL3*⁺ cholangiocytes with other cells (Fig. 6f and Additional file 1: Figs. S19, S20). The *ORMDL3*⁺ cholangiocytes showed relatively high communications with non-inflammatory macrophage and inflammatory monocyte/macrophages (Fig. 6f), recalling that these two types of immune cells have been remarkably enriched by PBC-risk genes in our above analysis. There were 35 significant ligand-receptor interactions (including source and target) of *ORMDL3*⁺ cholangiocytes were predicted, including MIF – (CD74 + CXCR4), MIF – (CD74 + CD44), VEGFA – VEGFR2, and NAMPT-INSR (Fig. 7a, b). There existed several unique ligand-receptor pairs in *ORMDL3*⁺ cholangiocytes





compared with *ORMDL3*⁻ cholangiocytes, including VEGFA-VEGFR2, VEGFA-VEGFR1R2 and VEGFA-VEGFR1 (Additional file 1: Fig. S21).

By performing a pattern recognition analysis based on the non-negative matrix factorization to uncover the global communication patterns among all cell populations, we observed that five communication patterns that connect cell populations with signaling pathways in the context of both outgoing signaling (i.e., treating cells as source, Fig. 8a) and incoming signaling (i.e., treating cells as target, Additional file 1: Fig. S22a), respectively. We found that a large portion of outgoing signaling of

ORMDL3⁺ cholangiocytes is characterized by pattern #1, which represents multiple signaling pathways, including MIF, PARs, VISFATIN, COMPLEMENT, ANGPTL, PROS, CHEMERIN, AGT, VEGF, and IGF (Fig. 8b). Compared with *ORMDL3*⁻ cholangiocytes, the VEGF signaling pathway is specific for *ORMDL3*⁺ cholangiocytes as source cells to interact with other cells (Fig. 8b). On the other hand, the communication patterns of both *ORMDL3*⁺ and *ORMDL3*⁻ cholangiocytes as target cells showed similar patterns (Additional file 1: Fig. S22b). Network centrality analysis confirmed that VEGF signaling pathway is not only a significant sender (i.e., source

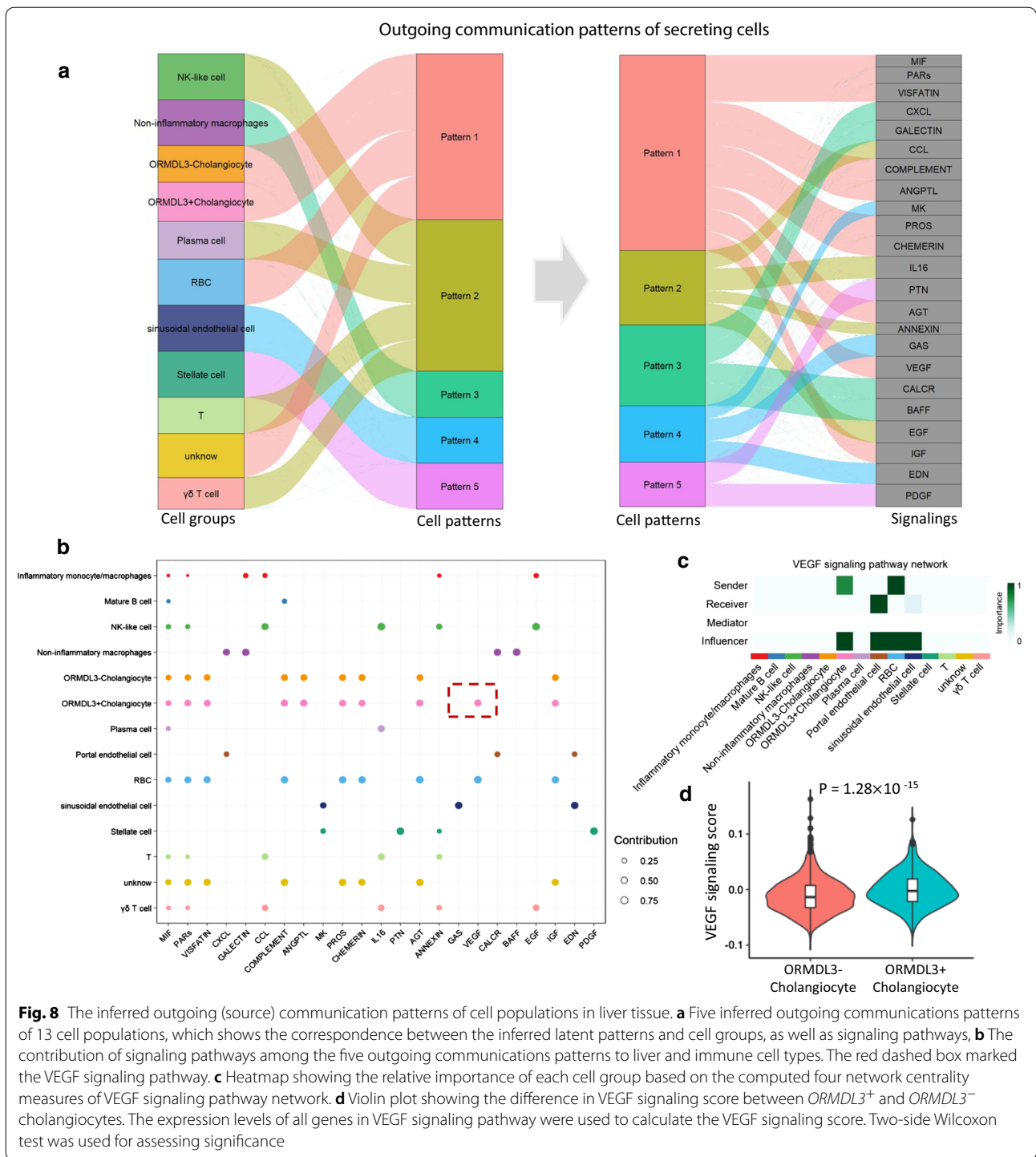


Fig. 8 The inferred outgoing (source) communication patterns of cell populations in liver tissue. **a** Five inferred outgoing communications patterns of 13 cell populations, which shows the correspondence between the inferred latent patterns and cell groups, as well as signaling pathways, **b** The contribution of signaling pathways among the five outgoing communications patterns to liver and immune cell types. The red dashed box marked the VEGF signaling pathway. **c** Heatmap showing the relative importance of each cell group based on the computed four network centrality measures of VEGF signaling pathway network. **d** Violin plot showing the difference in VEGF signaling score between *ORMDL3*⁺ and *ORMDL3*⁻ cholangiocytes. The expression levels of all genes in VEGF signaling pathway were used to calculate the VEGF signaling score. Two-side Wilcoxon test was used for assessing significance

cells) but also a prominent influencer controlling the communications for *ORMDL3*⁺ cholangiocytes (Fig. 8c). Notably, among all known ligand-receptor pairs, VEGF signaling pathway is dominated by VEGFA ligand and its VEGFR1 receptor (Additional file 1: Fig. S23). Using the expression levels of all genes in the VEGF signaling

pathway to calculate a VEGF activity score, we found that *ORMDL3*⁺ cholangiocytes exhibited a significantly higher activity score than that among *ORMDL3*⁻ cholangiocytes ($P = 1.28 \times 10^{-15}$, Fig. 8d). These results suggest that VEGF signaling pathway play an important role in cellular communications of *ORMDL3*⁺ cholangiocytes.

Discussion

Using an integrative genomics approach based on multiple layers of evidence, we identified that the genetics-influenced expression of 29 risk genes were remarkably associated with PBC. Among them, 10 genes, including *IRF5* [5, 6, 8, 9], *SOCS1* [5], *SYNGR1* [5, 7], *ORMDL3* [7, 9, 33], *MANBA* [5], *IDUA* [5], *DGKQ* [5], *FCRL3* [40], *NAAA* [41], and *SH2B3* [5], have been documented to be associated with PBC. There were 19 newly identified PBC-risk genes, such as *GSNK2B*, *LY6G5B*, *DDAH2*, *C6orf48*, and *HLA-DMA*. Some of these novel risk genes such as *DDAH2* and *HLA-DMA* have been reported to be associated with the autoimmune diseases, including type I diabetes [42], rheumatoid arthritis [43], and systemic lupus erythematosus [44]. The previously-reported gene of *ORMDL3* is related to biological functions of innate immune system and metabolism. Moreover, *ORMDL3* has also been extensively reported to be linked with other inflammatory diseases, including childhood asthma [45], inflammatory bowel diseases [38], rheumatoid arthritis [39], and Crohn's disease [46]. Functional enrichment analyses uncovered that these genetics-risk genes were notably enriched in several biological processes or disease-terms, which are relevant to autoimmune phenotypes [47, 48]. Together, these identified genes are more likely to be genuine genes implicated in PBC risk.

Our gene-property analysis unveiled that PBC-relevant genetic association signals were significantly enriched in several immune-related cell populations, including dendritic cells, T cells, and macrophage. Consistently, based on the genetic risk score, we revealed that these 29 PBC-associated genes were prominently enriched in non-inflammatory macrophage and inflammatory monocyte/macrophage. Dendritic cells have been shown to be relevant to the pathogenesis of PBC [19, 49]. Earlier studies have demonstrated that an intense biliary inflammatory CD8⁺ and CD4⁺ T cell response has been used for characterizing PBC [50]. Moreover, dendritic cells are crucial for inducing antigen-specific T-cell tolerance and for activating the self-specific T cells, which have central roles in many aspects of the pathogenesis of autoimmune liver diseases [51]. Macrophages and monocytes are key components of the innate immune system, and have tissue-repairing roles in reducing immune responses and enhancing tissue regeneration [52]. Multiple lines of evidence [53] have demonstrated that the infiltration of macrophages and monocytes in diseased tissues is considered to be a hallmark of several autoimmune diseases, including PBC [20, 54]. Recently, Dorris et al. [55] reported that the PBC susceptibility gene *C5orf30* modulates macrophage-mediated immune regulations. Overall, these results suggest that genetics-risk genes have

critical immuno-modulatory roles in the development of PBC.

To further examine the effects of liver cell populations and its immune microenvironments on PBC, we performed a regression-based polygenic analysis based on human liver tissues with immune cells. Cholangiocytes were significantly enriched by PBC-related genetic association signals. Previously, the non-parenchymal cholangiocytes have been reported to be injury in numerous human diseases termed as cholangiopathies [56], including PBC [56, 57]. Recently, Banales and coworkers [56] have demonstrated that cholangiocytes play pivotal roles in innate and adaptive immune responses relevant to immune-mediated cholangiopathies. Erice et al. [58] reported that microRNA-506 induces PBC-like features in human cholangiocytes and promotes the activating processes of immune responses. Moreover, we found that there existed higher metabolism activity score of cholangiocytes than other cells among liver tissues, indicating that abnormal metabolic pathways may involve in the etiology of PBC, which is in line with previous results [59]. Interestingly, the cell subset of *ORMDL3*⁺ cholangiocytes have strikingly higher metabolic activity than *ORMDL3* negative cells.

Compared with *ORMDL3*⁻ cholangiocytes, we found 77 significant DEGs among *ORMDL3*⁺ cholangiocytes, which contain numerous cytokine and chemokine genes, such as *CXCL8*, *CCL3*, and *CXCL1*, that may involve in mediating the immune-regulation for PBC risk. Furthermore, based on cellular communications analysis, we identified *ORMDL3*⁺ cholangiocytes exhibited high interactions with two innate immune cell types of non-inflammatory macrophage and inflammatory monocyte/macrophages. Several vital signaling pathways, including MIF, PARs, VEGF, and IGF, were predicted to implicate in the cellular interactions of *ORMDL3*⁺ cholangiocytes with other cells. The VEGF signaling pathway showed a higher specificity for *ORMDL3*⁺ cholangiocytes than *ORMDL3*⁻ cholangiocytes. VEGF is a potent stimulating factor for angiogenesis and vascular permeability, which have been reported to involve in PBC [60]. Multiple lines of evidence have demonstrated that VEGF has an important role in pathological conditions that are associated to autoimmune diseases, such as systemic lupus erythematosus, rheumatoid arthritis, inflammatory bowel disease, and multiple sclerosis [61].

There exist some limitations should be cautious. Although we leveraged integrated bioinformatics methods to highlight PBC-associated risk genes based on multiple omics data, there were many potential risk genes with suggestive evidence for PBC as shown in the supplemental tables needed to be further studied. Due to the heterogeneity across different datasets used in the

present investigation, we leveraged different statistical methods for multiple testing correction for each dataset, such as $FDR < 0.05$ for MAGMA-based gene association analysis and S-MultiXcan analysis, permuted $P < 0.05$ for genome-wide pathway enrichment analysis, Bonferroni corrected $P < 0.05$ for gene-property analysis, and empirical P value < 0.05 for in silico permutation analysis. In view of current integrative genomic analysis is only based on samples derived from European ancestries, more studies based on other ancestries should be performed to validate the effects of these risk genes on PBC.

Conclusions

In summary, current study provides multiple lines of evidence to support 29 genes including 19 novel genes are remarkably associated with PBC susceptibility. To the best of our knowledge, this is the first study to parse genetics-influenced human liver cell subpopulations and its immune microenvironments that contribute risk to PBC, and found that *ORMDL3*⁺ cholangiocytes potentially play important immune-regulatory roles in the pathogenesis of PBC. Current study gives several highlighted genetics-risk genes and disease-relevant cell types for unveiling the genetic mechanisms of PBC.

Methods

Datasets

1. *Single-cell transcriptomes of PBC* We downloaded two independent single cell RNA sequencing profiles (Accession number: GSE93170 and GSE115469) from the GEO database. With regard to the dataset of GSE93170, there were clinically and pathologically diagnosed six healthy controls and six PBC patients enrolled with written informed consent. Peripheral CD4⁺T cells were used to extract total RNA. The Agilent microarray of SurePrint G3 human GE 8 × 60 K microarray kit was leveraged to produce gene expression profiles according to manufacturer's protocols. The GSE115469 dataset contained five samples from primary liver patients, which were used for scRNA sequencing based on the 10 × Genomics Chromium Single Cell Kits. A total of 8444 parenchymal and non-parenchymal cells have obtained the transcriptional profiles based on the CellRanger analysis pipeline. The raw digital matrix of gene expression (namely UMI counts per gene per cell) was filtered, normalized and clustered. Cell was omitted if it has a very high (> 0.5) mitochondrial genome transcript ratio or a very small library size (< 1500).
2. *Bulk-based expression profiles of PBC* We also downloaded two independent bulk-based expression datasets based on liver tissue (Accession num-

ber: GSE159676) and blood (Accession number: GSE119600) from the Gene Expression Omnibus (GEO) database. The dataset of GSE159676 contained six healthy controls and three PBC cases based on fresh frozen liver tissue, which were obtained from explanted livers or diagnostic liver biopsies. The Affymetrix Human Gene 1.0-st array was leveraged to produce bulk-based liver expression profiles with 17,046 probes. With respect to the dataset of GSE119600, there were 47 healthy controls and 90 PBC patients with whole blood samples. The Illumina HumanHT-12 V4.0 expression beadchip was leveraged to produce bulk-based blood transcriptomes with 47,230 probes.

3. *GWAS summary statistics on PBC* We downloaded a GWAS summary dataset on PBC from the IEU open GWAS project (<https://gwas.mrcieu.ac.uk/>) [5]. There were 2764 PBC patients and 10,475 healthy controls based on European ancestry in this dataset used for performing a meta-analysis of GWAS signals. A standard quality control (QC) pipeline was applied to remove low-quality SNPs. The software package of MaCH [62] with the reference of HapMap3 CEU + TSI samples was implemented to perform a genome-wide imputation analysis. There were 1,124,241 SNPs with minor allele frequency > 0.005 and imputation quality score $R^2 > 0.5$ included in the current analyses.

Combination of GWAS summary statistics with scRNA-seq data for PBC

We leveraged a widely-used method of RolyRoly [63], which was designed to gain the effects of SNPs near protein-coding genes on cell types contributing to complex traits, to explore genetics-influenced liver cell types for PBC. The regression-based polygenic model was used in the RolyRoly to incorporate GWAS summary data with scRNA-seq data (i.e., GSE115469) for identifying PBC-associated liver cell subpopulations. Let $g(i)$ represents a given gene relevant to SNP i , $S_j = \{i : g(i) = j\}$ represents a given set with multiple SNPs relevant to the gene j , and β_{S_j} represents a PBC-GWAS-derived effect-size vector of S_j with a *priori* assumption that $\beta_{S_j} \sim \text{MVN}(0, \sigma_j^2 I_{|S_j|})$. Under the assumption, RolyPoly offers a polygenic linear model for β_{S_j} :

$$\sigma_j^2 = \gamma_0 + \sum_{i=1}^N \gamma_i \alpha_{ji}$$

where γ_0 represents an intercept term, $\alpha_{ji} (i = 1, 2, \dots, N)$ represents a group of annotations, for example, cell-type-specific gene expressions, and γ_i is the annotation's

coefficient for α_{ji} . To fit the observed and expected sum squared SNP effect sizes relevant to each gene, RolyPoly applies the method-of-moments estimators to estimate γ_i by the following formula:

$$E\left(\sum_{i \in S_j} \hat{\beta}_i^2\right) = \sigma_j^2 \text{Tr}(R_{S_j}^2) + |S_j| \sigma_e^2 n^{-1}$$

where R_{S_j} represents the linkage disequilibrium (LD) matrix of S_j . The 1000 Genome Project European Phase 3 panel [64] was used to calculate the LD among SNPs. The major histocompatibility complex (MHC) region was removed due to the highly extensive LD in this region. RolyPoly utilized the 1000 iterations of block bootstrap to assess standard errors for calculating t-statistic and corresponding P value. P value ≤ 0.05 was interpreted to be of significance.

Integrative genomic analysis of combining GWAS summary statistics with eQTL data

To highlight the functional risk genes whose expressions were significantly associated with PBC, we leveraged the S-PrediXcan tool [65] to combine GWAS summary data on PBC with eQTL data for liver and blood tissues from the GTEx Project (version 8) [66]. A MASHR-based prediction method with two linear regression models was used to estimate gene expression weights:

$$Y = \alpha_1 + X_l \beta_l + \varepsilon_1$$

$$Y = \alpha_2 + G_g \gamma_g + \varepsilon_2$$

where ε_1 and ε_2 are independent error terms, α_1 and α_2 are intercepts, Y is the n dimensional vector for n samples, X_l is the allelic dosage for SNP l in n samples, β_l is the effect size of SNP l , $G_g = \sum_{i \in \text{gene}(g)} \omega_{ig} X_i$ is the predicted expression calculated by ω_{ig} and X_i , in which ω_{ig} is derived from the GTEx Project, and γ_g is the effect size of G_g . The Wald-statistic Z score for each association is transformed as:

$$Z_g = \frac{\hat{\gamma}_g}{se(\hat{\gamma}_g)} \approx \sum_{i \in \text{gene}(g)} \omega_{ig} \frac{\hat{\sigma}_i}{\hat{\sigma}_g} \frac{\hat{\beta}_i}{se(\hat{\beta}_i)}$$

where $\hat{\sigma}_g$ is the standard deviation of G_g and can be calculated from the 1000 Genomes Project European Phase 3 Panel [64], $\hat{\beta}_i$ is the effect size from GWAS on PBC and $\hat{\sigma}_i$ is the standard deviation of $\hat{\beta}_i$.

To enhance the statistical power to identify significant genes whose expression has similar functions across different tissues, we leveraged the S-MultiXcan tool [21] to incorporate convergent evidence across 49 different

GTEx tissues. The S-MultiXcan fits a multivariate regression model from multiple tissue models jointly:

$$Y = \sum_{j=1}^p T_j g_j + e = Tg + e$$

where $\tilde{T}_j = \sum_{i \in \text{gene}(j)} \omega_i X_i$ is the predicted expression of tissue j , and T_j is the standardization of \tilde{T}_j to *mean* = 0 and *standarddeviation* = 1. g_j is the effect size for the predicted gene expression in tissue j , e is an error term with variance σ_e^2 , and p is the number of chosen tissues. There were 22,279 genes used in the multivariate regression model. $P < 6.89 \times 10^{-4}$ (FDR < 0.05) was considered to be significant.

Gene-based genetic association analysis

We conducted a gene-level association analysis of the GWAS summary statistics on PBC by leveraging a multivariate converging regression model in the Multi-marker Analysis of GenoMic Annotation (MAGMA) [32, 67]. The analyzed SNP set among each gene was depended on whether the SNP mapped into the body of the gene or its extended regions (± 20 kb downstream or upstream). The 1000 Genomes Project Phases 3 European Panel [64] was used to compute the LD between SNPs. The P value threshold was set to 0.0016, and the method of Benjamini–Hochberg false discovery rate (FDR) was applied for multiple testing correction [68]. Furthermore, to investigate the biological processes involved in PBC, we performed genome-wide pathway enrichment analysis using the *build-in* function of the MAGMA gene-set method [32]. The competitive P value of each pathway was computed by leveraging the results that the incorporated effect of genes in a given pathway are prominently larger than the incorporated effect of all rest genes. The *build-in* function of 10,000 permutations in MAGMA was used for adjusting competitive P values. We utilized the widely-used pathway resource of KEGG with latest version [69] for the MAGMA-based pathway enrichment analysis.

Multidimensional scaling analysis

To obtain the similarity of enriched pathways identified from MAGMA-based pathway enrichment analysis, we carried out a multidimensional scaling (MDS) analysis to group these biological pathways. First, we arranged a *pathway.txt* file included all the significant enriched pathways, and then utilized the Jaccard distance algorithm [70] to calculate the pathway-pathway distance scores according to overlapped genes. Using the distance scores among pathways, we obtained the first two components of results from the MDS analysis (i.e., MDS1 and MDS2). Subsequently, we plotted the clusters of these identified

pathways via MDS1 and MDS2 using the *symbols* function in R platform [71]. The most significant pathway (i.e., pathway has the lowest P value in each cluster) was used to mark each cluster.

In silico permutation analysis

We referenced the method used in previous studies [11, 67, 68, 72] to perform an in silico permutation analysis of 100,000 times of random selections (N_{Total}) for validating the consistency of results from S-MultiXcan analysis (Geneset #1, $N=308$, $FDR \leq 0.05$) with other results from three distinct analyses: MAGMA analysis (Geneset #2: $N=563$, $FDR \leq 0.05$), S-PrediXcan on liver (Geneset #3: $N=76$, $FDR \leq 0.05$), and S-PrediXcan on blood (Geneset #4: $N=115$, $FDR \leq 0.05$). First, we separately calculated the number of overlapped genes between Geneset #1 and Genesets #2, #3 and #4 ($N_{Observation}$). Second, we used the total number of genes in MAGMA, S-PrediXcan on liver, and S-PrediXcan on blood as the background genes ($N_{Background}=18,068$, 12,033, and 12,070, respectively). By randomly selecting the same number of genes as Genesets #2, #3, and #4 from the background genes to overlap with Geneset #1, we computed the number of overlapped genes in each time (N_{Random}). The empirical P value was calculated by using the formula: $P = \frac{N_{Random} \geq N_{Observation}}{N_{Total}}$. The empirically permuted P value ≤ 0.05 is interpreted as significance. By using the same method as above, we also performed an in silico permutation analysis for results from S-MultiXcan, MAGMA, and S-PrediXcan (on liver and blood) at a significant level of P value ≤ 0.05 to further explore the consistency.

Functional enrichment analysis of disease- and GO-terms

We conducted a disease-based enrichment analysis for these identified risk genes associated with PBC by using the WEB-based Gene SeT Analysis Toolkit (WebGestalt: <http://www.webgestalt.org>) [73] based on the GLAD4U database [74]. Moreover, we used the WebGestalt tool to perform a functional enrichment analysis for these common PBC-genetic risk genes based on the Gene Ontology (GO) database [75]. There were three categories of GO-terms: molecular function (MF), cellular component (CC), and biological process (BP). The number of genes in each GO-term is between 5 and 2000. The over-representation algorithm was adopted for evaluating the significant level for these enrichment analyses, and the Benjamini–Hochberg FDR method was used for multiple correction. In addition, the WebGestalt tool was used to conduct functional enrichment analyses for these significantly differentially expression genes (DEGs) between *ORMDL3*⁺ and *ORMDL3*⁻ cholangiocytes.

Protein–protein interaction network analysis

To explore the functional interactions of these identified PBC-associated genes, we conducted a protein–protein interaction (PPI) network-based analysis by leveraging the GeneMANIA tool (<http://www.genemania.org/>), which is a widely-used *plug-in* of Cytoscape platform [76–78]. By using PBC-associated genes as an input list, the GeneMANIA would predict genes with similar biological functions and construct interacted links by incorporating current existing genomics and proteomics information, containing co-expression associations and shared protein domains.

MAGMA gene-property analysis

To identify PBC-associated single cell subpopulations enriched by MAGMA-identified genes, we conducted MAGMA gene property analysis using the web-access tool of FUMA (<https://fuma.ctglab.nl/>) [79], which is a highly efficient and easy-to-use software, to integrate gene-level association signals from GWAS summary data on PBC [5] with scRNA-seq data based on liver tissue from the Mouse Cell Atlas [80]. There were 20 distinct cell types of liver tissue in the Mouse Cell Atlas. The Bonferroni method [81] was used for multiple testing correction.

Immune cell-specific expression quantitative trait loci

To find the eQTL for PBC-risk SNPs, we first extracted genetic variants statistics around upstream and downstream 400 kb of the targeted genes from GWAS summary data. We used the *LocusZoom* (<http://locuszoom.org/>) to figure a regional association plot for each gene. Then, we explored the cis-eQTL and promotor-interacting eQTL (pieQTL) among the Database of Immune Cell Expression quantitative trait loci and Epigenomics (DICE, <https://dice-database.org/landing>) [82] for annotating functional genetic variants.

Defining cell activity scores

We applied the cell activity score (CAS) to evaluate the immunological degree and metabolic activity of each cell type by using a pre-defined expression gene set [83]. The CASs were obtained by using a widely-used equation: $CAS_j(n) = \text{average [RLE (PGS}_j, n)] - \text{average [RLE (CGS}_m, n)]$, where PGS_j is a pre-curated gene set j in a given cell n , and CGS_m is a control gene set that was randomly selected from aggregate expression levels bins, which gain a comparable distribution of expression levels and over size to that of the pre-defined gene set. RLE represents the relative expression of PGS_j or CGS_m . The *AddModuleScore* function in the Seurat tool [84] was leveraged to calculate the

CAS with default parameters. We used pre-collected 85 metabolism-related pathways ($N=1667$ genes) in KEGG database [69], such as primary bile acid biosynthesis (ID: 00120), pyruvate metabolism (ID: 00620), and oxidative phosphorylation (ID: 00640), to define inflammatory score and metabolic activity score, respectively.

Cellular interactions among different cell types

To unveil potential cell-to-cell communications of *ORMDL3*⁺ and *ORMDL3*⁻ cholangiocytes with other liver and immune cells, we leveraged the CellChat R package [85] to infer the cellular interactions based on the normalized scRNA-seq dataset (i.e., GSE115469). The algorithm of CellChat could examine the ligand-receptor interactions significance among different types of cells based on the expression of soluble agonist, soluble antagonist, and stimulatory and inhibitory membrane-bound co-receptors. By summing the probabilities of the ligand-receptor interactions among a given signaling pathway, we could calculate the communication probability for the pathway.

Immunohistochemistry for the expression of *ORMDL3* in liver

Through searching the information retrieval system, we found four patients diagnosed as PBC through pathology in the past 2 years in the First Affiliated Hospital of Wenzhou Medical University, and three of them were able to obtain liver tissue sections. Approved by Ethics Committee in Clinical Research (ECCR) of the First Affiliated Hospital of Wenzhou Medical University, the liver paraffin sections of the PBC patients and paracarcinoma paraffin section of intrahepatic metastasis of rectal stromal tumor patient as negative control were used in this research. Immunohistochemistry was performed to assess the differential expression of *ORMDL3* in liver between PBC patient and normal control. Briefly, 5-mm paraffin sections were deparaffinized with xylene and then rehydrated through descending grades of alcohol. Antigen retrieval was performed by heating heated (95 °C) in the 0.01 M sodium citrate buffer (pH 6.0) for 15 min and incubating in 3% hydrogen peroxide for 10 min to block endogenous peroxidases. The paraffin-embedded liver sections were incubated overnight at 4 °C with Anti-*ORMDL3* antibody (Abcam, Cambridge, MA, USA), followed by the appropriate horseradish peroxidase-conjugated secondary antibodies (ZsBio, Beijing, China). Diaminobenzidine (DAB) was used as the chromogenic substrate and the sections were observed under the microscopy.

Statistical analysis

Differential gene expression (DGE) analyses between controls and PBC patients of three RNA expression datasets (i.e., GSE93170, GSE159676, and GSE119600) were examined by using the Student's T-test. P value ≤ 0.05 was of significance. We also performed a co-expression pattern analysis in the dataset of GSE93170 for genetics-risk genes among PBC and healthy controls to evaluate whether the co-expression patterns were changed due to the disease status. The PLINK (v1.90) [86] was used to calculate the LD values among SNPs. The hypergeometric test was used to evaluate the significant enrichment for the disease- and GO-term enrichment analysis. The Jaccard distance algorithm [70] was used to assess the similarities among pathways.

Abbreviations

PBC: Primary biliary cholangitis; GWAS: Genome-wide association study; SNP: Single nucleotide polymorphism; eQTL: Expression quantitative trait loci; DHS: DNase I-hypersensitive site; scRNA-seq: Single cell RNA sequencing; GEO: The gene expression omnibus; QC: Quality control; LD: Linkage disequilibrium; MHC: Major histocompatibility complex; MAGMA: The Multi-marker Analysis of GenoMic Annotation; FDR: False discovery rate; MDS: Multidimensional scaling; WebGestalt: The WEB-based Gene SeT Analysis Toolkit; GO: Gene ontology; MF: Molecular function; BP: Biological process; CC: Cellular component; DEG: Differential expression genes; PPI: Protein-protein interaction; pieQTL: Promoter-interacting expression quantitative loci; DICE: The database of immune cell expression quantitative trait loci and epigenomics; CAS: Cell activity score; PGS: Pre-curated gene set; CGS: Control gene set; RLE: Relative expression.

Supplementary Information

The online version contains supplementary material available at <https://doi.org/10.1186/s12951-021-01154-2>.

Additional File 1: Figure S1. Circus plot showing the results of gene-level genetic association analysis of GWAS summary statistics on PBC. **Figure S2.** MAGMA-based functional annotation analysis for GWAS summary data. **a)** MAGMA-based pathway enrichment analysis based on GWAS summary data on PBC. **b)** Multidimensional scaling analysis of 41 significant pathways identified MAGMA-based pathway analysis. **Figure S4.** Results of MAGMA gene-property analysis based on the web-access tool of FUMA. **Figure S2.** Venn plot shows the overlap of results between MAGMA and S-MultiXcan analysis. **Figure S5.** Permutation analysis of 100,000 times for results from MAGMA and S-PrediXcan (liver and blood) compared with results from S-MultiXcan across multiple tissues. **Figure S6.** Differential gene expression analysis of 29 risk genes based on bulk RNA profiles of liver tissue (Dataset of GSE159676). **Figure S7.** Differential gene expression analysis of 29 risk genes based on bulk RNA profiles of blood tissue (Dataset of GSE119600). **Figure S8.** Differential gene expression analysis of 29 risk genes based on bulk RNA profiles in CD4+T cells (Dataset of GSE93170). **Figure S9.** Functional characterization of 29 risk associated with PBC. **a)** Schematic diagram showing the literature mining and GWAS catalog searching for novel PBC-risk genes. **b)** Phenotype-based enrichment analysis based on the GLAD4U database for 29 risk genes. **Figure S10.** Functional enrichment analysis of GO-term of biological process for 29 PBC-risk genes. **Figure S11.** Functional enrichment analysis of GO-term of cellular components for 29 PBC-risk genes. **Figure S12.** Functional enrichment analysis of GO-term of molecular function for 29 PBC-risk genes. **Figure S13.** Gene-drug interaction analysis for these identified PBC-associated risk genes. **a)** Drug-gene interaction analysis showing 10 druggable gene categories. **b)** Drug-gene subnetwork. **Figure**

S14. Violin plot showing the difference in the expression level of *Ormdl3* between cholangitis-affected mice and healthy controls. **Figure S15.** The expression of *ORMDL3* examined in PBC livers and paracarcinoma of intrahepatic metastasis by immunohistochemistry. **Figure S16.** Box plots showing the effects of different genotypes (CC, CT, and TT) of rs9303277 on the expression of *ORMDL3* among different immune cell types. **Figure S17.** Functional enrichment analysis of differential expressed genes between *ORMDL3+* and *ORMDL3-* cholangiocytes. **Figure S18.** Identify signals contributing most to outgoing (sources) or incoming (targets) signaling of cell populations in liver tissues (GSE115469). **Figure S19.** The aggregated cell-to-cell communication network among cell populations in liver tissues (GSE115469). **Figure S20.** The cellular communications of *ORMDL3-* Cholangiocyte with other cell populations in liver tissues (GSE115469). **Figure S21.** Dot plots showing that predicted cellular interactions of *ORMDL3-* Cholangiocyte with other cell populations in liver tissues (GSE115469). **Figure S22.** The inferred incoming (target) communication patterns of cell populations in liver tissue (GSE115469). **Figure S23.** Relative contribution of each ligand-receptor pair to that of VEGF signaling pathway.

Additional File 2: Table S1. Summary of collected datasets in current integrative genomics analysis. **Table S2.** Significant genes identified from MAGMA-based gene association analysis (FDR < 0.05). **Table S3.** MAGMA-identified significant enriched pathways based on GWAS summary data. **Table S4.** MAGMA gene-property analysis identifies liver single cells based on the Mouse Cell Atlas. **Table S5.** Significant PBC-associated genes identified by the S-MultiXcan tool. **Table S6.** Significant genes identified from S-PrediXcan analysis by integrating GWAS summary data with GTEx liver eQTL data. **Table S7.** Significant genes identified from S-PrediXcan analysis by integrating GWAS summary data with GTEx blood eQTL data. **Table S8.** Phenotype-based enrichment analysis of these 29 identified risk genes for PBC based on the GLAD4U database. **Table S9.** PBC-associated risk genes matched in druggable gene categories. **Table S10.** Results of PBC-associated liver cell types by using RolyPolybased integrative analysis of combining GWAS summary data with scRNA-seq data. **Table S11.** The percentage of expressed 27 genetic risk genes in all 13 distinct cell types in human liver tissues. **Table S12.** The significantly upregulated DEGs among *ORMDL3+* cholangiocytes. **Table S13.** The significantly down-regulated DEGs among *ORMDL3+* cholangiocytes. **Table S14.** Significantly KEGG pathways enriched by up-regulated DEGs among *ORMDL3+* cholangiocytes using the clusterProfiler tool. **Table S15.** Significantly KEGG pathways enriched by down-regulated DEGs among *ORMDL3+* cholangiocytes using the clusterProfiler tool. **Table S16.** GO enrichment analysis according to biological process terms for 71 down-regulated DEGs among *ORMDL3+* cholangiocytes. **Table S17.** GO enrichment analysis according to cellular component terms for 71 down-regulated DEGs among *ORMDL3+* cholangiocytes. **Table S18.** GO enrichment analysis according to molecular function terms for 71 downregulated DEGs among *ORMDL3+* cholangiocytes.

Acknowledgements

We appreciate Cordell and his colleagues who have deposited and shared GWAS summary data on primary biliary cirrhosis in the IEU open GWAS project. We also thank to all authors who have deposited single cell RNA sequencing data and bulk-based RNA expression data on primary biliary cirrhosis in the NCBI GEO database.

Authors' contributions

YM and ML conceived and designed the study. YM, BX, CD, FQ, SL, YZ, and JL contributed to management of data collection. YM, BX, CD, FQ, JL, HZ, XL, and YH, conducted bioinformatics analysis and data interpretation. YM, JS, and ML wrote the manuscripts. All authors reviewed and approved the final manuscript. All authors read and approved the final manuscript.

Funding

This study was funded by the Scientific Research Foundation for Talents of Wenzhou Medical University (KYQD20201001 to Y.M.).

Availability of data and materials

All the GWAS summary data applied in the present analysis can be obtained from the IEU open GWAS project (<https://gwas.mrcieu.ac.uk/>). The GTEx eQTL data (version 8) can be gained from the Zenodo repository (<https://zenodo.org/record/3518299#Xv6Z6igzbg1>). The single cell RNA sequencing data and bulk-based RNA expression data were downloaded from the NCBI GEO database (<https://www.ncbi.nlm.nih.gov/gds/>). All scripts used in the Methods are deposited in the public available GitHub repository: https://github.com/mayunlong89/PBC_project.

Declarations

Ethics approval and consent to participate

Not applicable.

Consent for publication

All authors are agreed to publish this paper.

Competing interests

The authors declare no conflict of interest.

Author details

¹Department of Infectious Diseases, The First Affiliated Hospital of Wenzhou Medical University, Wenzhou 325000, Zhejiang, China. ²School of Life Science and Technology, Harbin Institute of Technology, Harbin 150080, China. ³Institute of Biomedical Big Data, School of Ophthalmology and Optometry and Eye Hospital, School of Biomedical Engineering, Wenzhou Medical University, Wenzhou 325027, Zhejiang, China. ⁴State Key Laboratory for Diagnosis and Treatment of Infectious Diseases, The First Affiliated Hospital, Collaborative Innovation Center for Diagnosis and Treatment of Infectious Diseases, Zhejiang University School of Medicine, Hangzhou 310003, Zhejiang, China. ⁵Wenzhou Institute, University of Chinese Academy of Sciences, Wenzhou 325011, Zhejiang, China.

Received: 19 September 2021 Accepted: 21 November 2021

Published online: 06 December 2021

References

1. Beuers U, Gershwin ME, Gish RG, Invernizzi P, Jones DE, Lindor K, Ma X, Mackay IR, Parés A, Tanaka A, et al. Changing nomenclature for PBC: from 'cirrhosis' to 'cholangitis'. *J Hepatol.* 2015;63(5):1285–7.
2. Lindor KD, Bowlus CL, Boyer J, Levy C, Mayo M. Primary biliary cholangitis: 2018 practice guidance from the American association for the study of liver diseases. *Hepatology.* 2019;69(1):394–419.
3. Rong G, Zhong R, Lleo A, Leung PS, Bowlus CL, Yang GX, Yang CY, Coppel RL, Ansari AA, Cuevas DA, et al. Epithelial cell specificity and epitope recognition by serum autoantibodies in primary biliary cirrhosis. *Hepatology.* 2011;54(1):196–203.
4. Tanaka A, Leung PSC, Gershwin ME. The genetics of primary biliary cholangitis. *Curr Opin Gastroenterol.* 2019;35(2):93–8.
5. Cordell HJ, Han Y, Mellis GF, Li Y, Hirschfield GM, Greene CS, Xie G, Juran BD, Zhu D, Qian DC, et al. International genome-wide meta-analysis identifies new primary biliary cirrhosis risk loci and targetable pathogenic pathways. *Nat Commun.* 2015;6:8019.
6. Hirschfield GM, Liu X, Xu C, Lu Y, Xie G, Lu Y, Gu X, Walker EJ, Jing K, Juran BD, et al. Primary biliary cirrhosis associated with HLA, IL12A, and IL12RB2 variants. *N Engl J Med.* 2009;360(24):2544–55.
7. Qiu F, Tang R, Zuo X, Shi X, Wei Y, Zheng X, Dai Y, Gong Y, Wang L, Xu P, et al. A genome-wide association study identifies six novel risk loci for primary biliary cholangitis. *Nat Commun.* 2017;8:14828.
8. Liu X, Invernizzi P, Lu Y, Kosoy R, Lu Y, Bianchi I, Podda M, Xu C, Xie G, Macchiardi F, et al. Genome-wide meta-analyses identify three loci associated with primary biliary cirrhosis. *Nat Genet.* 2010;42(8):658–60.
9. Mellis GF, Floyd JA, Morley KI, Cordell HJ, Franklin CS, Shin SY, Heneghan MA, Neuberger JM, Donaldson PT, Day DB, et al. Genome-wide association study identifies 12 new susceptibility loci for primary biliary cirrhosis. *Nat Genet.* 2011;43(4):329–32.

10. Juran BD, Hirschfield GM, Invernizzi P, Atkinson EJ, Li Y, Xie G, Kosoy R, Ransom M, Sun Y, Bianchi I, et al. Immunochip analyses identify a novel risk locus for primary biliary cirrhosis at 13q14, multiple independent associations at four established risk loci and epistasis between 1p31 and 7q32 risk variants. *Hum Mol Genet.* 2012;21(23):5209–21.
11. Ma Y, Huang Y, Zhao S, Yao Y, Zhang Y, Qu J, Wu N, Su J. Integrative Genomics Analysis Reveals a 21q22.11 Locus Contributing Risk to COVID-19. *Hum Mol Genet.* 2021;30(12):2109–21.
12. Zhu Z, Zhang F, Hu H, Bakshi A, Robinson MR, Powell JE, Montgomery GW, Goddard ME, Wray NR, Visscher PM, et al. Integration of summary data from GWAS and eQTL studies predicts complex trait gene targets. *Nat Genet.* 2016;48(5):481–7.
13. Pickrell JK. Joint analysis of functional genomic data and genome-wide association studies of 18 human traits. *Am J Hum Genet.* 2014;94(4):559–73.
14. Finucane HK, Bulik-Sullivan B, Gusev A, Trynka G, Reshef Y, Loh PR, Anttila V, Xu H, Zang C, Farh K, et al. Partitioning heritability by functional annotation using genome-wide association summary statistics. *Nat Genet.* 2015;47(11):1228–35.
15. Zhang Y, Ma Y, Huang Y, Zhang Y, Jiang Q, Zhou M, Su J. Benchmarking algorithms for pathway activity transformation of single-cell RNA-seq data. *Comput Struct Biotechnol J.* 2020;18:2953–61.
16. Zhang F, Wei K, Slowikowski K, Fonseka CY, Rao DA, Kelly S, Goodman SM, Tabechian D, Hughes LB, Salomon-Escoto K, et al. Defining inflammatory cell states in rheumatoid arthritis joint synovial tissues by integrating single-cell transcriptomics and mass cytometry. *Nat Immunol.* 2019;20(7):928–42.
17. Corridoni D, Chapman T, Antanaviciute A, Satsangi J, Simmons A. Inflammatory bowel disease through the lens of single-cell RNA-seq technologies. *Inflamm Bowel Dis.* 2020;26(11):1658–68.
18. Nehar-Belaid D, Hong S, Marches R, Chen G, Bolisetty M, Baisch J, Walters L, Punaro M, Rossi RJ, Chung CH, et al. Mapping systemic lupus erythematosus heterogeneity at the single-cell level. *Nat Immunol.* 2020;21(9):1094–106.
19. Hiasa Y, Akbar SM, Abe M, Michitaka K, Horiike N, Onji M. Dendritic cell subtypes in autoimmune liver diseases; decreased expression of HLA DR and CD123 on type 2 dendritic cells. *Hepatol Res.* 2002;22(4):241–9.
20. Harada K, Shimoda S, Ikeda H, Chiba M, Hsu M, Sato Y, Kobayashi M, Ren XS, Ohta H, Kasashima S, et al. Significance of periductal Langerhans cells and biliary epithelial cell-derived macrophage inflammatory protein-3 α in the pathogenesis of primary biliary cirrhosis. *Liver Int.* 2011;31(2):245–53.
21. Barbeira AN, Pividori M, Zheng J, Wheeler HE, Nicolae DL, Im HK. Integrating predicted transcriptome from multiple tissues improves association detection. *PLoS Genet.* 2019;15(11):e1007889.
22. Hu HJ, Jin EH, Yim SH, Yang SY, Jung SH, Shin SH, Kim WU, Shim SC, Kim TG, Chung YJ. Common variants at the promoter region of the APOM confer a risk of rheumatoid arthritis. *Exp Mol Med.* 2011;43(11):613–21.
23. Tomer Y, Dolan LM, Kahaly G, Divers J, D'Agostino RB Jr, Imperatore G, Dabelea D, Marcovina S, Black MH, Pihoker C, et al. Genome wide identification of new genes and pathways in patients with both autoimmune thyroiditis and type 1 diabetes. *J Autoimmun.* 2015;60:32–9.
24. Mitchell AL, Attwood TK, Babbitt PC, Blum M, Bork P, Bridge A, Brown SD, Chang HY, El-Gebali S, Fraser MI, et al. InterPro in 2019: improving coverage, classification and access to protein sequence annotations. *Nucleic Acids Res.* 2019;47(D1):D351–d360.
25. Wang Q, Diskin S, Rappaport E, Attiyeh E, Mosse Y, Shue D, Seiser E, Jagannathan J, Shusterman S, Bansal M, et al. Integrative genomics identifies distinct molecular classes of neuroblastoma and shows that multiple genes are targeted by regional alterations in DNA copy number. *Cancer Res.* 2006;66(12):6050–62.
26. von Spee-Mayer C, Siebert E, Abdirama D, Rose A, Klaus A, Alexander T, Enghard P, Sawitzki B, Hiepe F, Radbruch A, et al. Low-dose interleukin-2 selectively corrects regulatory T cell defects in patients with systemic lupus erythematosus. *Ann Rheum Dis.* 2016;75(7):1407–15.
27. Atkinson MA, Eisenbarth GS, Michels AW. Type 1 diabetes. *Lancet.* 2014;383(9911):69–82.
28. Sundin DJ, Wolin MJ. Aldesleukin therapy in HIV-infected patients. *Am J Health Syst Pharm.* 1998;55(14):1520–3.
29. Heine A, Held SA, Daecke SN, Wallner S, Jayanarayana SP, Kurts C, Wolf D, Brossart P. The JAK-inhibitor ruxolitinib impairs dendritic cell function in vitro and in vivo. *Blood.* 2013;122(7):1192–202.
30. Zhou T, Kyritsi K, Wu N, Francis H, Yang Z, Chen L, O'Brien A, Kennedy L, Ceci L, Meadows V, et al. Knockdown of vimentin reduces mesenchymal phenotype of cholangiocytes in the Mdr2(-/-) mouse model of primary sclerosing cholangitis (PSC). *EBioMedicine.* 2019;48:130–42.
31. Ronca V, Mancuso C, Milani C, Carbone M, Oo YH, Invernizzi P. Immune system and cholangiocytes: a puzzling affair in primary biliary cholangitis. *J Leukoc Biol.* 2020;108(2):659–71.
32. de Leeuw CA, Mooij JM, Heskes T, Posthuma D. MAGMA: generalized gene-set analysis of GWAS data. *PLoS Comput Biol.* 2015;11(4):e1004219.
33. Nakamura M, Nishida N, Kawashima M, Aiba Y, Tanaka A, Yasunami M, Nakamura H, Komori A, Nakamura M, Zeniya M, et al. Genome-wide association study identifies TNFSF15 and POU2AF1 as susceptibility loci for primary biliary cirrhosis in the Japanese population. *Am J Hum Genet.* 2012;91(4):721–8.
34. Das S, Miller M, Broide DH. Chromosome 17q21 genes ORMDL3 and GSDMB in asthma and immune diseases. *Adv Immunol.* 2017;135:1–52.
35. Rydzynski Moderbacher C, Ramirez SI, Dan JM, Grifoni A, Hastie KM, Weiskopf D, Belanger S, Abbott RK, Kim C, Choi J, et al. Antigen-specific adaptive immunity to SARS-CoV-2 in acute COVID-19 and associations with age and disease severity. *Cell.* 2020;183(4):996–1012.e1019.
36. Su Y, Chen D, Yuan D, Lausted C, Choi J, Dai CL, Voillet V, Duvvuri VR, Scherler K, Troisch P, et al. Multi-omics resolves a sharp disease-state shift between mild and moderate COVID-19. *Cell.* 2020;183(6):1479–1495.e1420.
37. Unterholzner L, Keating SE, Baran M, Horan KA, Jensen SB, Sharma S, Sirois CM, Jin T, Latz E, Xiao TS, et al. IFI16 is an innate immune sensor for intracellular DNA. *Nat Immunol.* 2010;11(11):997–1004.
38. Liu JZ, van Sommeren S, Huang H, Ng SC, Alberts R, Takahashi A, Ripke S, Lee JC, Jostins L, Shah T, et al. Association analyses identify 38 susceptibility loci for inflammatory bowel disease and highlight shared genetic risk across populations. *Nat Genet.* 2015;47(9):979–86.
39. Kurreeman FA, Stahl EA, Okada Y, Liao K, Diogo D, Raychaudhuri S, Freudenberg J, Kochi Y, Patsopoulos NA, Gupta N, et al. Use of a multi-ethnic approach to identify rheumatoid arthritis-susceptibility loci, 1p36 and 17q12. *Am J Hum Genet.* 2012;90(3):524–32.
40. Tanaka A, Ohira H, Kikuchi K, Nezu S, Shibuya A, Bianchi I, Podda M, Invernizzi P, Takikawa H. Genetic association of Fc receptor-like 3 polymorphisms with susceptibility to primary biliary cirrhosis: ethnic comparative study in Japanese and Italian patients. *Tissue Antigens.* 2011;77(3):239–43.
41. Zamanou A, Samiotaki M, Panayotou G, Margaritis L, Lymberi P. Fine specificity and subclasses of IgG anti-actin autoantibodies differ in health and disease. *J Autoimmun.* 2003;20(4):333–44.
42. Fogarty RD, Abhary S, Javadiyan S, Kasmeridis N, Petrovsky N, Whiting MJ, Craig JE, Burdon KP. Relationship between DDAH gene variants and serum ADMA level in individuals with type 1 diabetes. *J Diabetes Complications.* 2012;26(3):195–8.
43. Morel J, Roch-Bras F, Molinari N, Sany J, Eliaou JF, Combe B. HLA-DMA*0103 and HLA-DMB*0104 alleles as novel prognostic factors in rheumatoid arthritis. *Ann Rheum Dis.* 2004;63(12):1581–6.
44. Yen JH, Chen CJ, Tsai WC, Tsai JJ, Ou TT, Liu HW. HLA-DMA and HLA-DMB genotyping in patients with systemic lupus erythematosus. *J Rheumatol.* 1999;26(9):1930–3.
45. Moffatt MF, Kabesch M, Liang L, Dixon AL, Strachan D, Heath S, Depner M, von Berg A, Bufe A, Rietschel E, et al. Genetic variants regulating ORMDL3 expression contribute to the risk of childhood asthma. *Nature.* 2007;448(7152):470–3.
46. Barrett JC, Hansoul S, Nicolae DL, Cho JH, Duerr RH, Rioux JD, Brant SR, Silverberg MS, Taylor KD, Barmada MM, et al. Genome-wide association defines more than 30 distinct susceptibility loci for Crohn's disease. *Nat Genet.* 2008;40(8):955–62.
47. Grayson PC, Kaplan MJ. At the Bench: neutrophil extracellular traps (NETs) highlight novel aspects of innate immune system involvement in autoimmune diseases. *J Leukoc Biol.* 2016;99(2):253–64.

48. Mo X, Guo Y, Qian Q, Fu M, Lei S, Zhang Y, Zhang H. Mendelian randomization analysis revealed potential causal factors for systemic lupus erythematosus. *Immunology*. 2020;159(3):279–88.
49. Kita H, Lian ZX, Van de Water J, He XS, Matsumura S, Kaplan M, Luketic V, Coppel RL, Ansari AA, Gershwin ME. Identification of HLA-A2-restricted CD8(+) cytotoxic T cell responses in primary biliary cirrhosis: T cell activation is augmented by immune complexes cross-presented by dendritic cells. *J Exp Med*. 2002;195(1):113–23.
50. Coppel RL, Gershwin ME. Primary biliary cirrhosis: the molecule and the mimic. *Immunol Rev*. 1995;144:17–49.
51. Swiecki M, Colonna M. The multifaceted biology of plasmacytoid dendritic cells. *Nat Rev Immunol*. 2015;15(8):471–85.
52. Ma WT, Gao F, Gu K, Chen DK. The role of monocytes and macrophages in autoimmune diseases: a comprehensive review. *Front Immunol*. 2019;10:1140.
53. Carlsen HS, Baekkevold ES, Morton HC, Haraldsen G, Brandtzaeg P. Monocyte-like and mature macrophages produce CXCL13 (B cell-attracting chemokine 1) in inflammatory lesions with lymphoid neogenesis. *Blood*. 2004;104(10):3021–7.
54. Peng A, Ke P, Zhao R, Lu X, Zhang C, Huang X, Tian G, Huang J, Wang J, Invernizzi P, et al. Elevated circulating CD14(low)CD16(+) monocyte subset in primary biliary cirrhosis correlates with liver injury and promotes Th1 polarization. *Clin Exp Med*. 2016;16(4):511–21.
55. Dorris ER, Tazzyman SJ, Moylett J, Ramamoorthi N, Hackney J, Townsend M, Muthana M, Lewis MJ, Pitzalis C, Wilson AG. The autoimmune susceptibility gene C5orf30 regulates macrophage-mediated resolution of inflammation. *J Immunol*. 2019;202(4):1069–78.
56. Banalles JM, Huebert RC, Carlsen T, Strazzabosco M, LaRusso NF, Gores GJ. Cholangiocyte pathobiology. *Nat Rev Gastroenterol Hepatol*. 2019;16(5):269–81.
57. Lleo A, Maroni L, Glaser S, Alpini G, Marziani M. Role of cholangiocytes in primary biliary cirrhosis. *Semin Liver Dis*. 2014;34(3):273–84.
58. Erice O, Munoz-Garrido P, Vaquero J, Perugorria MJ, Fernandez-Barrena MG, Saez E, Santos-Laso A, Arbelaz A, Jimenez-Agüero R, Fernandez-Irigoyen J, et al. MicroRNA-506 promotes primary biliary cholangitis-like features in cholangiocytes and immune activation. *Hepatology*. 2018;67(4):1420–40.
59. Bell LN, Wulff J, Comerford M, Vuppalanchi R, Chalasani N. Serum metabolic signatures of primary biliary cirrhosis and primary sclerosing cholangitis. *Liver Int*. 2015;35(1):263–74.
60. Medina J, Sanz-Cameno P, García-Buey L, Martín-Vilchez S, López-Cabrera M, Moreno-Otero R. Evidence of angiogenesis in primary biliary cirrhosis: an immunohistochemical descriptive study. *J Hepatol*. 2005;42(1):124–31.
61. Carvalho JF, Blank M, Shoenfeld Y. Vascular endothelial growth factor (VEGF) in autoimmune diseases. *J Clin Immunol*. 2007;27(3):246–56.
62. Li Y, Willer CJ, Ding J, Scheet P, Abecasis GR. MaCH: using sequence and genotype data to estimate haplotypes and unobserved genotypes. *Genet Epidemiol*. 2010;34(8):816–34.
63. Calderon D, Bhaskar A, Knowles DA, Golan D, Raj T, Fu AQ, Pritchard JK. Inferring relevant cell types for complex traits by using single-cell gene expression. *Am J Hum Genet*. 2017;101(5):686–99.
64. Auton A, Brooks LD, Durbin RM, Garrison EP, Kang HM, Korbel JO, Marchini JL, McCarthy S, McVean GA, Abecasis GR. A global reference for human genetic variation. *Nature*. 2015;526(7571):68–74.
65. Barbeira AN, Dickinson SP, Bonazzola R, Zheng J, Wheeler HE, Torres JM, Torstenson ES, Shah KP, Garcia T, Edwards TL, et al. Exploring the phenotypic consequences of tissue specific gene expression variation inferred from GWAS summary statistics. *Nat Commun*. 2018;9(1):1825.
66. The Genotype-Tissue Expression (GTEx) project. *Nat Genet* 2013; 45(6):580–585.
67. Xu M, Li J, Xiao Z, Lou J, Pan X, Ma Y. Integrative genomics analysis identifies promising SNPs and genes implicated in tuberculosis risk based on multiple omics datasets. *Aging (Albany NY)*. 2020;12(19):19173–220.
68. Ma X, Wang P, Xu G, Yu F, Ma Y. Integrative genomics analysis of various omics data and networks identify risk genes and variants vulnerable to childhood-onset asthma. *BMC Med Genomics*. 2020;13(1):123.
69. Kanehisa M, Goto S. KEGG: kyoto encyclopedia of genes and genomes. *Nucleic Acids Res*. 2000;28(1):27–30.
70. Ma Y, Li J, Xu Y, Wang Y, Yao Y, Liu Q, Wang M, Zhao X, Fan R, Chen J, et al. Identification of 34 genes conferring genetic and pharmacological risk for the comorbidity of schizophrenia and smoking behaviors. *Aging (Albany NY)*. 2020;12(3):2169–225.
71. Zhong Y, Chen L, Li J, Yao Y, Liu Q, Niu K, Ma Y, Xu Y. Integration of summary data from GWAS and eQTL studies identified novel risk genes for coronary artery disease. *Medicine (Baltimore)*. 2021;100(11):e24769.
72. Dong Z, Ma Y, Zhou H, Shi L, Ye G, Yang L, Liu P, Zhou L. Integrated genomics analysis highlights important SNPs and genes implicated in moderate-to-severe asthma based on GWAS and eQTL datasets. *BMC Pulm Med*. 2020;20(1):270.
73. Wang J, Duncan D, Shi Z, Zhang B. WEB-based GEne SeT Analysis Toolkit (WebGestalt): update 2013. *Nucleic Acids Res*. 2013;41:W77–83.
74. Jourquin J, Duncan D, Shi Z, Zhang B. GLAD4U: deriving and prioritizing gene lists from PubMed literature. *BMC Genomics*. 2012;13(Suppl 8):S20.
75. Gene Ontology Consortium: going forward. *Nucleic Acids Res* 2015; 43(Database issue):D1049–1056.
76. Warde-Farley D, Donaldson SL, Comes O, Zuberi K, Badrawi R, Chao P, Franz M, Grouios C, Kazi F, Lopes CT, et al. The GeneMANIA prediction server: biological network integration for gene prioritization and predicting gene function. *Nucleic Acids Res*. 2010;38:W214–220.
77. Shannon P, Markiel A, Ozier O, Baliga NS, Wang JT, Ramage D, Amin N, Schwikowski B, Ideker T. Cytoscape: a software environment for integrated models of biomolecular interaction networks. *Genome Res*. 2003;13(11):2498–504.
78. Ma Y, Li MD. Establishment of a strong link between smoking and cancer pathogenesis through DNA methylation analysis. *Sci Rep*. 2017;7(1):1811.
79. Watanabe K, Umičević Mirkov M, de Leeuw CA, van den Heuvel MP, Posthuma D. Genetic mapping of cell type specificity for complex traits. *Nat Commun*. 2019;10(1):3222.
80. Han X, Wang R, Zhou Y, Fei L, Sun H, Lai S, Saadatpour A, Zhou Z, Chen H, Ye F, et al. Mapping the mouse cell atlas by microwell-seq. *Cell*. 2018;172(5):1091–1107.e1017.
81. Etymology: Bonferroni correction. *Emerg Infect Dis* 2015; 21(2):289.
82. Chandra V, Bhattacharyya S, Schmiedel BJ, Madrigal A, Gonzalez-Colin C, Fotsing S, Crinklaw A, Seumois G, Mohammadi P, Kronenberg M, et al. Promoter-interacting expression quantitative trait loci are enriched for functional genetic variants. *Nat Genet*. 2021;53(1):110–9.
83. Ren X, Wen W, Fan X, Hou W, Su B, Cai P, Li J, Liu Y, Tang F, Zhang F, et al. COVID-19 immune features revealed by a large-scale single-cell transcriptome atlas. *Cell*. 2021;184(7):1895–1913.e1819.
84. Butler A, Hoffman P, Smibert P, Papalexi E, Satija R. Integrating single-cell transcriptomic data across different conditions, technologies, and species. *Nat Biotechnol*. 2018;36(5):411–20.
85. Jin S, Guerrero-Juarez CF, Zhang L, Chang I, Ramos R, Kuan CH, Myung P, Plikus MV, Nie Q. Inference and analysis of cell-cell communication using cell chat. *Nat Commun*. 2021;12(1):1088.
86. Chang CC, Chow CC, Tellier LC, Vattikuti S, Purcell SM, Lee JJ. Second-generation PLINK: rising to the challenge of larger and richer datasets. *Gigascience*. 2015;4:7.

Publisher's Note

Springer Nature remains neutral with regard to jurisdictional claims in published maps and institutional affiliations.

Ready to submit your research? Choose BMC and benefit from:

- fast, convenient online submission
- thorough peer review by experienced researchers in your field
- rapid publication on acceptance
- support for research data, including large and complex data types
- gold Open Access which fosters wider collaboration and increased citations
- maximum visibility for your research: over 100M website views per year

At BMC, research is always in progress.

Learn more biomedcentral.com/submissions

